Cerebral Cortex April 2008;18:846-867
doi:10.1093/cercor/bhm116
Advance Access publication July 21, 2007

Observer-Independent Cytoarchitectonic Mapping of the Human Superior Parietal Cortex

Filip Scheperjans[1,2], Klaudia Hermann[1,2], Simon B. Eickhoff[1], Katrin Amunts[1,3], Axel Schleicher[2] and Karl Zilles[1,2]

[1]Institute of Medicine, Research Center Jülich and Brain Imaging Center West, D-52425 Jülich, Germany, [2]C. and O. Vogt Institute for Brain Research, University of Düsseldorf, D-40001 Düsseldorf, Germany and [3]Department of Psychiatry and Psychotherapy, Aachen University Hospital, D-52074 Aachen, Germany

The human superior parietal cortex (SPC; Brodmann areas [BA] 5 and 7) comprises the superior parietal lobule and medial wall of the intraparietal sulcus (mIPS) laterally and the posterior paracentral lobule and precuneus medially. Receptor autoradiographic and functional studies indicate more complex segregations in the SPC than suggested by Brodmann (1909). Differences to other historical maps may be due to anatomical variability between brains and different definition criteria for areas. To provide a reliable anatomical reference of the SPC, we performed an observer-independent cytoarchitectonic mapping of this region in 10 human postmortem brains. Cytoarchitecture was analyzed in cell-body–stained brain sections using gray-level index profiles. Multivariate statistical analysis of profile shape allowed the exact localization of cytoarchitectonic borders and quantification of interareal differences. We identified 3 areas in BA 5 (5L, 5M, and 5Ci), 4 in BA 7 (7PC, 7A, 7P, and 7M), and 1 in the anterior mIPS (hIP3). Locations of their borders relative to macroanatomical landmarks varied considerably between brains and hemispheres. Cytoarchitectonic profiles of areas 5Ci and hIP3 differed most from those of the remaining areas, and differences between subareas were stronger in BA 5 than in BA 7. These areas are possible structural correlates of functional segregations within the SPC.

Keywords: area 5, area 7, brain mapping, intraparietal sulcus (IPS), precuneus, superior parietal lobule (SPL)

Introduction

The human superior parietal cortex (SPC) can be macroanatomically subdivided (Fig. 1) into 2 lateral parts, the superior parietal lobule (SPL) and the medial wall of the intraparietal sulcus (mIPS), and 2 medial parts, the posterior part of the paracentral lobule (PCL) and the precuneus (PrC). In Brodmann's cytoarchitectonic map, the SPC comprises 2 main areas (Fig. 2): 1) Brodmann area (BA) 5 in the anterior SPL near the vertex and on the posterior part of the PCL and 2) BA 7 occupying the larger posterior part of the SPL and the PrC (Brodmann 1909). Later Brodmann introduced a subdivision of BA 7 into anterior BA 7a and posterior BA 7b (Brodmann 1914).

Further structural heterogeneity within human SPC has recently been described using quantitative receptor autoradiography (Scheperjans, Grefkes, et al. 2005; Scheperjans, Palomero-Gallagher, et al. 2005). Distinct distribution patterns of receptor-binding sites of different neurotransmitter systems revealed 3 subareas within BA 5 (areas 5L, 5M, and 5Ci; Scheperjans, Grefkes, et al. 2005). Moreover, the distribution patterns of neurotransmitter receptors in the anterior SPC were similar to those of somatosensory areas, whereas the patterns in the posterior SPC resembled those of the extrastriate visual cortex (Scheperjans, Palomero-Gallagher, et al. 2005).

These structural findings are in line with results from functional imaging experiments, which showed complex segregations in human SPC. Different activations were observed during reaching movements depending on somatosensory (anterior SPL) or visual (posterior SPL) guidance and on the location of the target in the visual field (central vs. peripheral/anterior medial wall of the intraparietal sulcus [amIPS] vs. posterior SPL; Prado et al. 2005; Wenderoth et al. 2006). Furthermore, distinct activations in the parietal lobe were reported during grasping (anterior lateral wall of the intraparietal sulcus) and reaching (amIPS, SPL, and PrC; Grefkes et al. 2002, 2004; Culham et al. 2006). The PCL is implicated in somatosensory and motor related processing and plays an important role in micturition control (Richer et al. 1993; Lim et al. 1994; Allison et al. 1996; Sakakibara et al. 1999).

Functional imaging studies usually correlate cortical activations with Brodmann's map (1909, 1914) using its 3-dimensional representation in the atlas of Talairach and Tournoux (1988) as an anatomical reference. This work, however, is derived from visual cytoarchitectonic inspection of a single human postmortem brain (Brodmann 1909). Several other cyto- and myeloarchitectonic maps of the SPC show considerably different areal patterns with a total number of areas ranging from 3 to 34 (see Discussion for details; Table 1; Figs. 2 and 3; Vogt 1911; von Economo and Koskinas 1925; Gerhardt 1940; Sarkisov et al. 1955; Batsch 1956).

Such profound differences may be caused by different subjective mapping criteria and staining techniques used by different investigators. Another important factor may be the interindividual anatomical variability between brains that is not accounted for in these studies (Zilles et al. 2002, 2003; Uylings et al. 2005). For the human brain, it has been repeatedly demonstrated that the size and location of cytoarchitectonic areas varies considerably between individuals even for primary sensory areas like area 3b and BA 17 (Geyer et al. 1999; Amunts et al. 2000). The exact position of cytoarchitectonic borders between areas cannot be derived from macroscopical anatomical landmarks like sulci or gyri (Geyer et al. 1996, 1999; Amunts et al. 1999; Grefkes et al. 2001; Morosan et al. 2001; Zilles et al. 2002; Uylings et al. 2005; Caspers et al. 2006; Choi et al. 2006; Eickhoff, Schleicher, et al. 2006; Malikovic et al. 2007; Rottschy et al. 2007).

All historical microanatomical maps of the human parietal cortex have a common drawback, which is the lack of information about the cortex within the intraparietal sulcus (IPS; Brodmann 1909, 1914; Vogt 1911; von Economo and Koskinas 1925; Gerhardt 1940; Sarkisov et al. 1955; Batsch 1956). However, anatomical and functional studies in nonhuman primates and human brains have revealed several

distinct cortical areas within this sulcus (Grefkes et al. 2002, 2004; Grefkes and Fink 2005; Choi et al. 2006; Culham et al. 2006; Iacoboni 2006; Orban et al. 2006; Fig. 4). In the human brain, using observer-independent cytoarchitectonic mapping, areas hIP1 and hIP2 have been recently identified in the fundus and lateral wall of the anterior IPS, which may be homologues of macaque areas AIP (anterior intraparietal area) and VIP (ventral intraparietal area; Choi et al. 2006). In macaques, the mIPS contains areas PEip (PE intraparietal, the rostral part of area PEa of Pandya and Seltzer [1982]) and MIP (medial intraparietal area; Matelli et al. 1998; Grefkes and Fink 2005). However, no cytoarchitectonic mapping of the human mIPS is available yet.

Consequently, for the investigation of structure-function relationships, there is a need for an anatomical reference of the human SPC that is uninfluenced by observer bias and that accounts for interindividual variability (Eickhoff et al. 2005). In this study, we present such a reference using an observer-independent technique for the delineation and characterization of cytoarchitectonic areas based on the statistical analysis of the laminar cell-body distribution in sections of postmortem brains (Schleicher et al. 1999, 2000, 2005; Amunts and Zilles 2001; Zilles et al. 2002). This method has been extensively tested and applied for several cortical regions including sensory and motor areas (Geyer et al. 1996, 1999; Amunts et al. 2000; Grefkes et al. 2001; Morosan et al. 2001; Eickhoff, Schleicher, et al. 2006; Malikovic et al. 2007; Rottschy et al. 2007) as well as association areas (Caspers et al. 2006; Choi et al. 2006). The interindividual variability was assessed by analyzing the cytoarchitecture of each area in 10 brains. This data can be used to create a probabilistic map of the SPC in stereotaxic space (Amunts and Zilles 2001; Mazziotta et al. 2001).

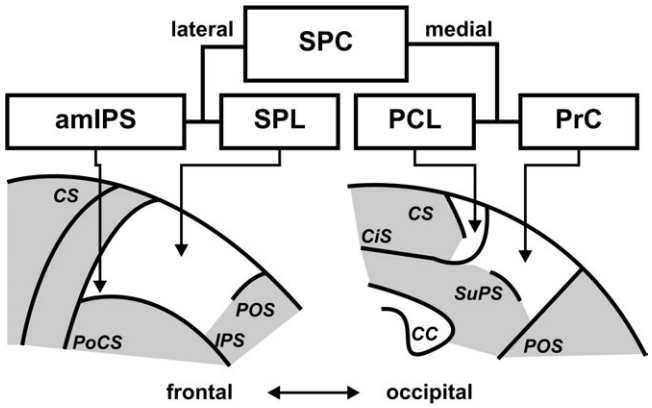

Figure 1. Schematic drawing of the lateral and medial aspects of a human hemisphere focused on the parietal region. The topography of the 4 different examined macroanatomical parts of the SPC (white area) is demonstrated: SPL, amIPS, posterior PCL, and PrC. CC, corpus callosum; CS, central sulcus. CiS, cingulate sulcus; IPS, intraparietal sulcus; PoCS, postcentral sulcus; POS, parieto-occipital sulcus; SuPS, subparietal sulcus.

Table 1
Comparison between our parcellation and those of previous studies (Figs. 2, 3, and 18)

Present study	Brodmann (1909, 1914)	von Economo and Koskinas (1925)	Sarkisov (1955)	Vogt (1911)	Gerhardt (1940)	Batsch (1956)
5Ci	5	PA_2	5	75	75scm	75sup
5M	5	PA_2	5	75	75	75sup
5L	5	PA_2	7	75	75	75inf
7PC	7a	PE_m	7	86/87	86/87	86
7A	7/7a	PE_m	7	83	83	83
7P	7/7b	PE_p/PE_γ	7a	85	85	85
7M	7	PE_p/PE_γ	7a	84	84	84
hIP3	7a	PD/PE(D)	7	86	86/87	86/87

Note: sup, superior; inf, inferior; scm, sulcus callosomarginalis (cingulate sulcus; Gerhardt 1940).

Materials and Methods

Histological Processing

Twelve human postmortem brains (Table 2; 6 male, 6 female, age range 37–86 years) were obtained from the Body Donor Program of the Anatomical Institute of the University of Düsseldorf from subjects with no clinical history of neurological or psychiatric diseases (Fig. 5*A*). The brains had been removed from the skull less than 24 h postmortem and fixed for approximately 6 months in formalin or in Bodian's fixative. During fixation, the brains were suspended at the basilar artery to avoid compression or distortion. The whole brains were embedded in paraffin and serially sectioned (thickness = 20 μm) in a coronal (11 brains) or sagittal (1 brain) plane (Fig. 5*B*). Each 15th section was stained for cell bodies using a modified silver staining method (Merker 1983). Every 60th coronal section (45th sagittal section) underwent analysis, resulting in a distance between examined sections of 1.2 mm or 0.9 mm, respectively.

Due to artifacts in the histological sections of some brains, the sample analyzed for area 7M differed from that of the other areas. Eight brains were analyzed with respect to all areas, 2 were analyzed for area 7M only, and 2 were analyzed for all areas except area 7M (Table 2). Thus, each area was mapped in 10 brains.

Observer-Independent Delineation of Cytoarchitectonic Borders

Borders between areas were identified using the method introduced by Schleicher et al. (1999, 2000, 2005; Fig. 5 *B*-*G*). Rectangular regions of interest (ROIs) were defined in the histological sections and scanned in a meander-like sequence with a CCD camera (XC-75, Sony, Japan) and a microscope (Universal, Zeiss, Germany) equipped with a computer-controlled motorized stage at an in-plane resolution of 1.05 μm per pixel (Fig. 5*B*). Images were processed using the KS 400 image analyzing software (Version 3.0, Zeiss). The gray-level index (GLI; Schleicher and Zilles 1990), estimating the volume fraction of cell bodies (Wree et al. 1982), was measured by adaptive thresholding in continuously adjoining square measuring fields (16 × 16 μm). In the resulting GLI image, each pixel represents the local volume fraction of cell bodies in the corresponding measuring field (Fig. 5*C*).

In each GLI image (i.e., ROI), the outer (between layers I and II) and inner (between layer VI and the white matter) cortical contours were interactively traced using in house software (MATLAB, The MathWorks, Inc., Natick, MA). The contour lines defined the start (outer contour) and end (inner contour) points of curvilinear traverses (spacing = 100 μm), which were calculated using a physical model based on electric field lines (Jones et al. 2000; Fig. 5*D*). Curvilinear traverses offer the best available solution because they follow the distortions of the cortical

Table 2
Brains used for cytoarchitectonic analysis of the SPC

Brain number	Sex	Age (years)	Cause of death	Plane of sectioning
146/86	Male	37	Right heart failure	Coronal
16/96[a]	Male	54	Myocardial infarction	Coronal
189/92[b]	Male	56	Rectal carcinoma	Coronal
2/95	Female	85	Mesenteric infarction	Coronal
207/84	Male	75	Toxic glomerulonephritis	Coronal
2431	Male	39	Drowning	Coronal
281/93	Male	69	Vascular disease	Coronal
340/83[b]	Female	79	Cardiorespiratory failure	Sagittal
544/91[a]	Female	79	Bladder carcinoma	Coronal
56/94	Female	72	Renal failure	Coronal
68/95	Female	79	Cardiorespiratory failure	Coronal
71/86	Female	86	Cardiorespiratory failure	Coronal

[a]Analyzed for area 7M only.
[b]Not analyzed for area 7M.

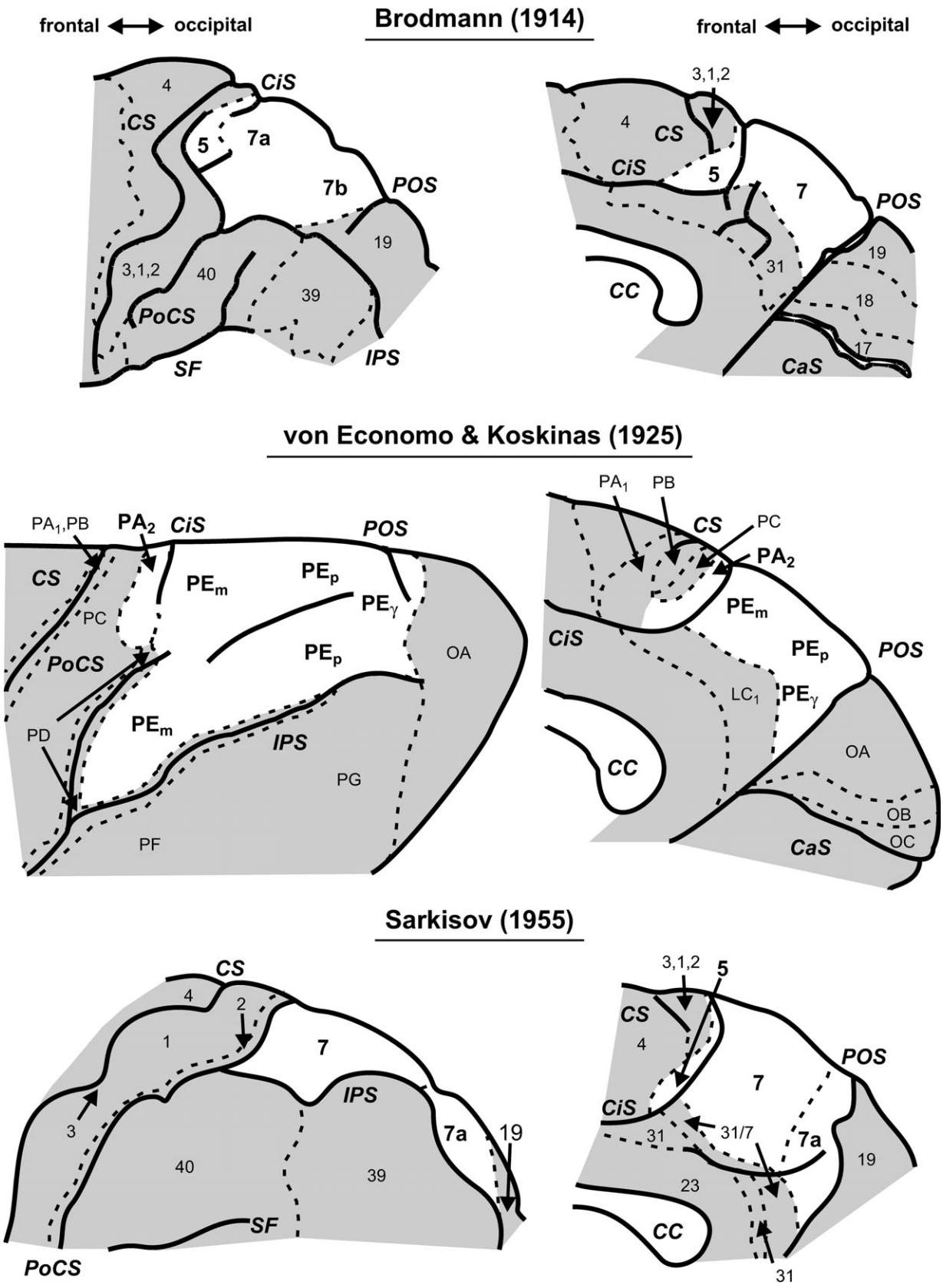

Figure 2. Modified schematic drawings of the lateral/dorsal (left) and medial (right) aspects of the maps of Brodmann (1914), von Economo and Koskinas (1925), and Sarkisov (1955) with emphasis on their parcellations of the SPC (white area). Dashed lines indicate the borders of the cortical areas. CaS, calcarine sulcus; CC, corpus callosum; CS, central sulcus; SF, sylvian fissure.

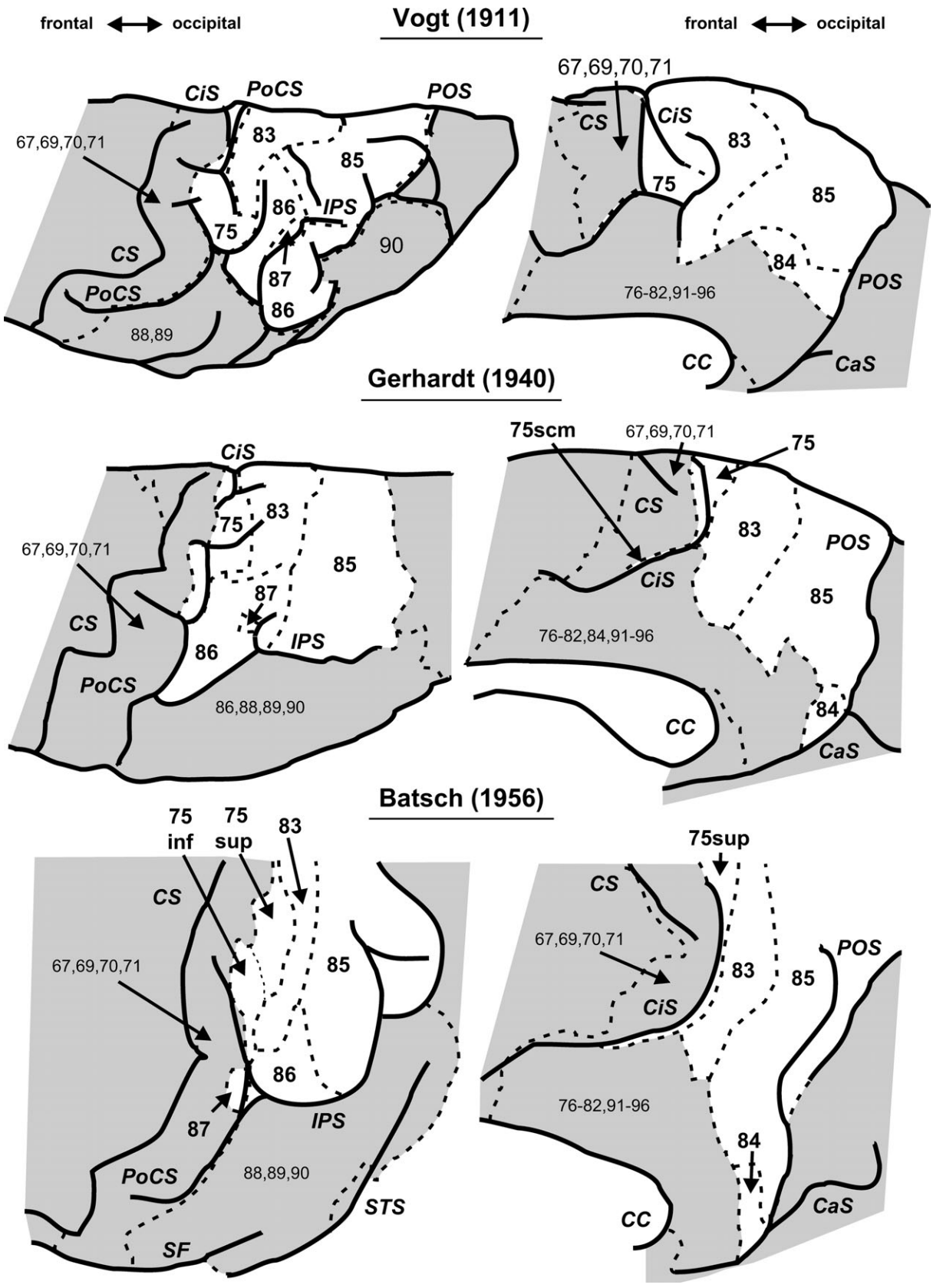

Figure 3. Modified schematic drawings of the lateral/dorsal (left) and medial (right) aspects of the maps of Vogt (1911), Gerhardt (1940), and Batsch (1956) with emphasis on their parcellations of the SPC (white area). Dashed lines indicate the borders of the main cortical areas. CaS, calcarine sulcus; CC, corpus callosum; CS, central sulcus; SF, sylvian fissure; STS, superior temporal sulcus.

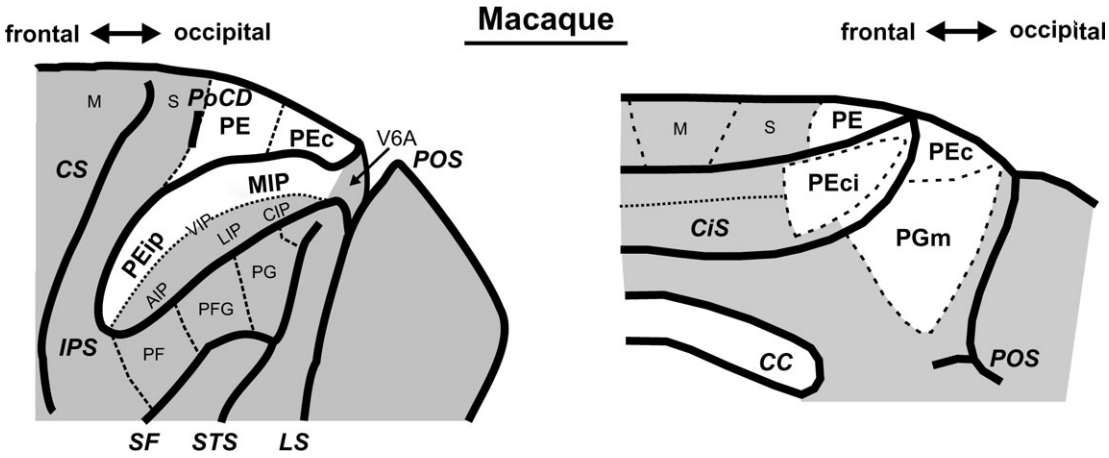

Figure 4. Schematic drawing of the commonly used parcellation of the macaque SPC (white area; lateral aspect = left, medial aspect = right; the IPS and CiS are opened). The map is an adaptation based on the drawings of Pandya and Seltzer (1982) and Grefkes and Fink (2005). Dashed lines indicate borders of the cortical areas if they have been published, and dotted lines correspond to the fundi of the opened sulci. CC, corpus callosum; CS, central sulcus; LS, lunate sulcus; M, primary motor cortex; PoCD, postcentral dimple; S, primary somatosensory cortex; SF, sylvian fissure; STS, superior temporal sulcus.

minicolumns caused by cortical folding and cross the cortical layers more perpendicularly than straight lines, especially in strongly gyrified cortex (Schleicher et al. 2005). GLI values were extracted along the course of the traverses from the surface to the white matter (= GLI profile). To compensate for variations in cortical thickness, each profile was resampled with linear interpolation to a standard length corresponding to a cortical thickness of 100% (0% = border between layers I and II; 100% = border to the white matter; Fig. 6). The profile shape was described using a 10-dimensional feature vector, composed of the mean amplitude and the first 4 statistical moments of both the profile and the absolute of its first differential quotient (Schleicher et al. 2000; Zilles et al. 2002).

Differences between the feature vectors, that is, between the shapes of the profiles, reflected differences in cytoarchitecture and were quantified using the Mahalanobis distance (MD; Mahalanobis et al. 1949; Schleicher et al. 2000). Distances were calculated between feature vectors from 2 abutting blocks of b (= block size) adjacent profiles to increase the signal-to-noise ratio. Blocks of profiles were analyzed in a sliding window of size $2b$, which was moved along the cortical ribbon with single-profile increments. The dependency of the MD between profile blocks on the window position was described by the MD function (Fig. 5*E*). Maxima of the distance function are expected to occur at positions where the sliding window is centered over a border between adjacent cortical areas and were tested for significance using a Hotelling's T^2 statistic with Bonferroni correction (Schleicher et al. 1999; Fig. 5*E*). A significant maximum was further processed if no higher maximum was found within one block size on either side. This sliding window procedure was repeated for block sizes $8 \leqslant b \leqslant 24$, and the significant maxima at different block sizes were plotted as a function of the window position (Fig. 5*F*). The frequency of significant maxima at each window position was determined and those borders further processed that had a frequency of at least 4 and no neighboring border with a higher frequency within an interval of 37 profiles on either side (a window of about twice the average cortical thickness; Fig. 5*G*). This threshold for accepting a cytoarchitectonic border was set relatively low because the cytoarchitectonic differences within the SPC were expected to be very subtle. This increased the risk of detection of false-positive borders caused by artifacts (e.g., blood vessels). However, all detected borders were microscopically verified and only accepted if they were reproducible in several adjacent sections (Figs. 7–9).

Statistical Analysis of Cytoarchitecture Using GLI Profiles

For each delineated cytoarchitectonic area, a sample of representative GLI profiles was extracted from 3–5 cortical ROIs per hemisphere (on average 34 profiles per ROI), which were free of histological artifacts, minimally curved, and orthogonally cut. The ROIs were systematically sampled within the whole extent of each area in order to represent all parts equally. A mean profile was calculated for each ROI.

The shape of each GLI profile is not influenced only by the laminar cytoarchitectonic pattern that is specific for the respective area. Confounding factors can be specific for the individual brain (e.g., global cell packing density) or specific for each ROI (e.g., distortions of the laminar pattern, i.e., of the relative width of each cortical layer, caused by cortical folding; von Economo and Koskinas 1925; Bok and von Kip 1936).

We separated the effect of global cell packing density from that of area-specific laminar cytoarchitecture by normalizing all profiles by dividing them by their mean GLI value (Eickhoff et al. 2007). To eliminate the effects of cortical folding, we used piecewise linear width normalization (PLWN) for the normalized mean GLI profiles (Eickhoff et al. 2007; Fig. 6). First, the cortical depths of the interlaminar borders were determined for each ROI using a semiautomatic method based on the superimposition of its mean GLI profile and the respective cytoarchitectonic section (Eickhoff et al. 2007). The basic principle was the detection of the steepest local increases/decreases of the profile curve (i.e., turning points), which occur at the transition between layers with relatively high GLI (layers II, IV, and VI) and layers with relatively low GLI (layers III and V; Figs. 10–13). A similar approach has been applied earlier by Amunts et al. (1995). The cortical depths of the interlaminar borders were then averaged across areas, hemispheres, and brains resulting in one overall pattern of interlaminar borders. For each ROI, the profile segments of the mean profile between the interlaminar borders were linearly stretched or shrunk to match this template (Eickhoff et al. 2007). The preservation of cytoarchitectonic profile information by PLWN is illustrated in Figure 6 where a mean profile across hemispheres and 10 brains is shown for area hIP3. In the "raw" mean profile, the variance in the relative width of each cortical layer between the ROIs of the same area leads to a blurred representation of the area's specific laminar cytoarchitecture. In the PLWN-corrected mean profile, the laminar cytoarchitectonic pattern is represented in more detail, as can be seen by comparison with Figure 13. Consequently, for each area, the resulting mean-normalized, PLWN-corrected GLI profile represents its specific laminar cytoarchitectonic pattern.

Dissimilarity of cytoarchitecture was quantified by calculating the Euclidean distance (ED) between the GLI profiles and tested for significance using permutation tests (Eickhoff et al. 2007; MATLAB, The MathWorks, Inc.). Because no significant interhemispheric differences in the shape of these profiles were found ($P > 0.05$), profiles were averaged across hemispheres for the analysis of interareal differences (significance level $P < 0.05$; family wise error corrected). The dissimilarity of the cytoarchitecture between the areas was visualized using multidimensional scaling (MDS; Fig. 14; SYSTAT 10.1, SPSS Inc., San Jose, CA). For visualization of the specific differences in the laminar pattern between selected areas, difference profiles were calculated for each brain by subtraction of 2 mean profiles and subsequently averaged across brains (Fig. 15).

The mean GLI of the profiles provides valuable information about cytoarchitectonic differences between areas. It was analyzed separately

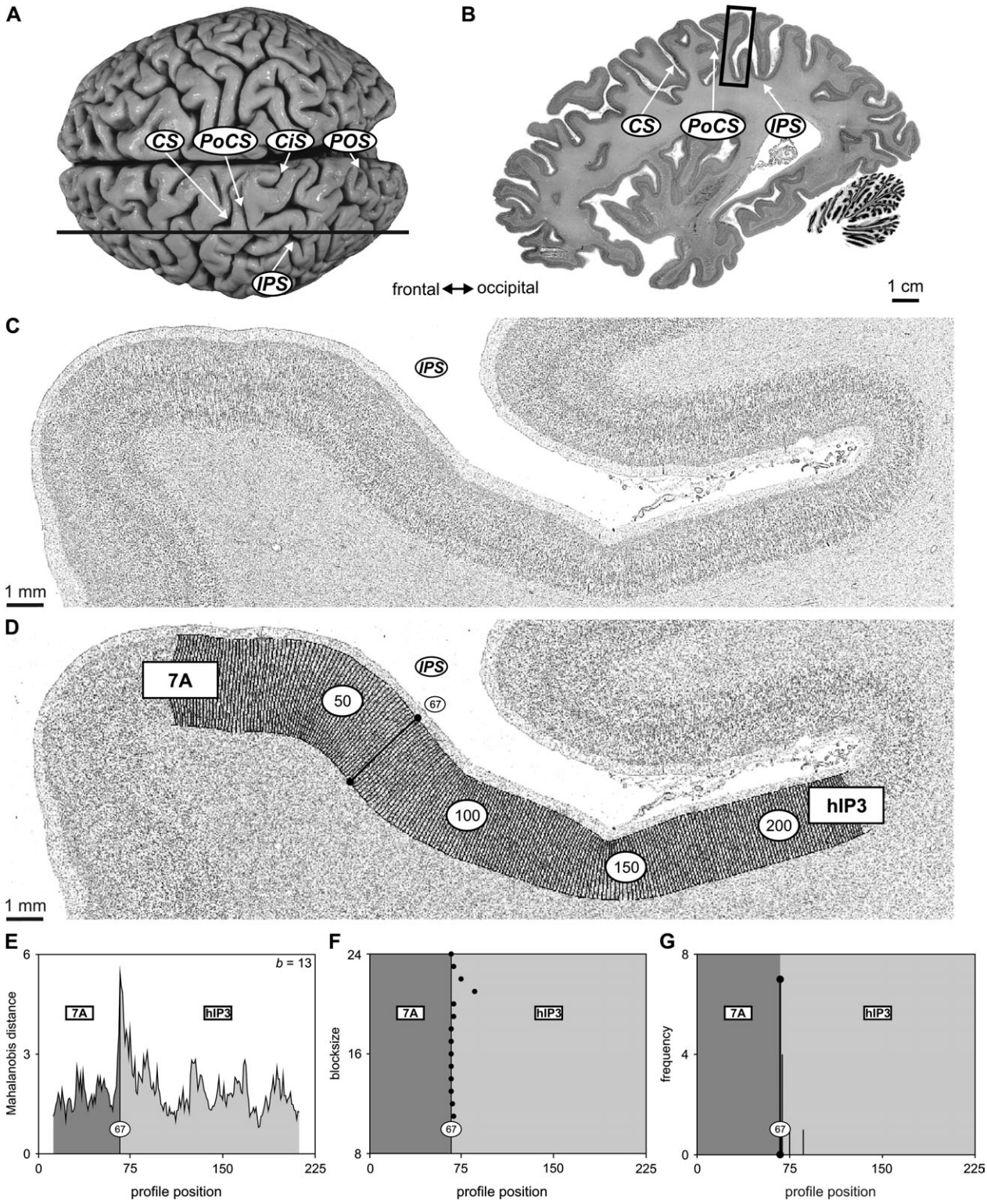

Figure 5. Image acquisition and observer-independent definition of cytoarchitectonic borders. (*A*) Dorsal view of one of the fixed human brains before sectioning. The black line corresponds to the level of the section in (*B*). (*B*) Sagittal cell-body–stained brain section (thickness = 20 μm) from the level depicted in (*A*). The area in the black square corresponds to one of the examined ROIs from that section (amIPS). (*C*) GLI image of the ROI depicted in *B* (amIPS). Gray values correspond to the volume fraction of cell bodies (dark = high volume fraction). (*D*) GLI image with contour lines and superimposed numbered curvilinear traverses along which the GLI profiles were extracted. The bar at profile position 67 corresponds to the significant maxima of the MD function in *E*–*G* caused by the cytoarchitectonic border between areas 7A and hIP3 as confirmed by microscopical examination. (*E*) MD function with a significant maximum at profile position 67. (*F*) Dependence of the position of significant maxima of the MD function (black dots) on the block size. Most dots are aligned at profile position 67. (*G*) Corresponding frequency of significant maxima at different profile positions across block sizes 8 → 24. The highest frequency occurred at profile position 67, which was selected as the putative cytoarchitectonic border between areas 7A and hIP3. CS, central sulcus.

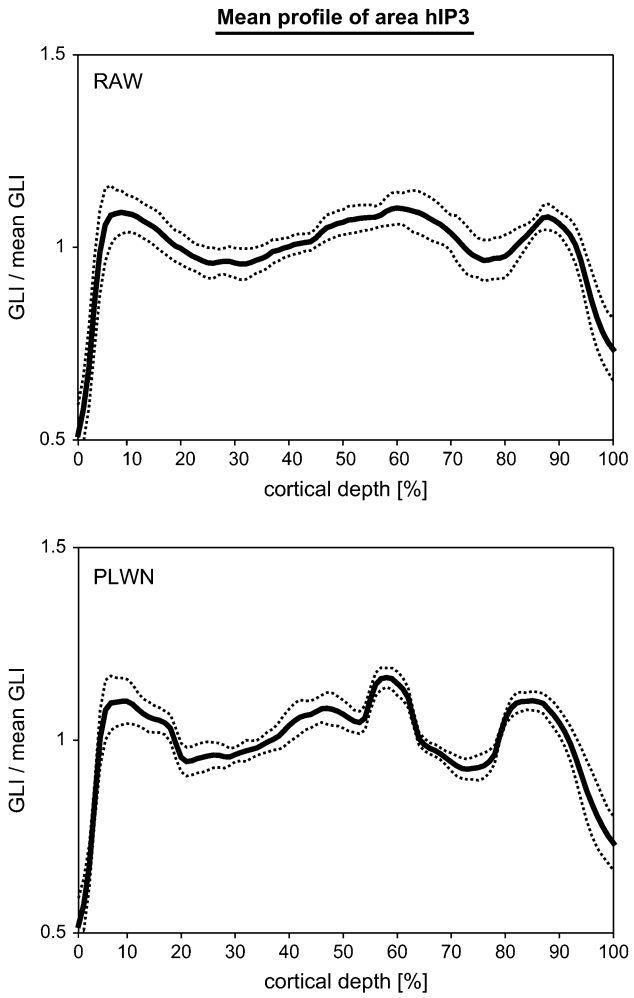

Figure 6. Comparison of the mean-normalized GLI profile of area hIP3 averaged across both hemispheres without (RAW) and with (PLWN) normalization of interlaminar borders prior to averaging. Dotted lines correspond to the standard deviation ($n = 10$).

from the profile shape (see above). No significant correlation between age and the mean GLI was found for any area ($P > 0.05$; Bonferroni corrected for multiple comparisons; mean Fisher's z from both hemispheres $\bar{z} = 0.20 \pm 0.14$ corresponding to mean Pearson's correlation coefficient $\bar{r} = 0.20$). Interhemispheric differences in mean GLI were tested for significance using analysis of variance (ANOVA; blocking factor: brain; Fig. 16). Because no significant differences were found ($P > 0.05$), interareal differences were tested using ANOVA (blocking factor: brain) with values averaged from both hemispheres (significance level $P < 0.05$; Bonferroni corrected for multiple comparisons).

No significant correlation between age and laminar width was found for any area or layer ($P > 0.05$; Bonferroni corrected for multiple comparisons; $\bar{z} = 0.39 \pm 0.30$; $\bar{r} = 0.37$). For each area, the differences of the width of the cortical layers between hemispheres were tested for significance using multivariate analysis of variance (MANOVA) with hemispheres as within factor and layers as main factor (blocking factor: brain). Because no interhemispheric differences were found ($P > 0.05$), the test for interareal differences was performed using values averaged from both hemispheres (Fig. 17). Global interareal differences were first tested for homogeneity using MANOVA (blocking factor: brain) with brain regions as main factor and layers as dependent variables to protect the overall significance level. Because the null hypothesis was excluded ($P < 0.05$; Bonferroni corrected for multiple comparisons), differences between areas for each layer were subsequently tested with ANOVA (significance level $P < 0.05$; Bonferroni corrected for multiple comparisons).

Analysis of Topographical Relations

Topographical relations were visually determined in the histological sections separately for each hemisphere. The analysis was focused on the location of the areas and of their borders with respect to anatomical landmarks. These landmarks included the lateral and medial brain surface, crowns of major gyri, and both walls and the fundi of major sulci. To look for an effect of the hemisphere on the location of the areas/borders, we tested for the independence between the hemisphere and the probability with which each area/border was found at a particular landmark using two-by-two contingency tables and Fisher's exact test (2-tailed; significance level $P < 0.05$). For significant interdependencies, we calculated odds ratios (OR) and their 95% confidence intervals (CI) if no cell had a probability of zero.

Results

The human SPC and amIPS consist of granular isocortex. Eight areas were reliably distinguished in this region by differences in cytoarchitecture: 3 in the region of BA 5 (5L, 5M, and 5Ci), 4 in the region of BA 7 (7PC, 7A, 7P, and 7M), and 1 in the amIPS (hIP3).

Observer-Independent Delineation of Cytoarchitectonic Borders

Figures 7–9 depict representative ROIs showing cytoarchitectonic borders in cell-body–stained sections and corresponding plots showing significant maxima of the MD function indicating the location of these borders. Figures 10–13 show the respective areas at higher magnification as well as mean profiles of the areas across hemispheres and brains. Because these profiles were PLWN corrected for each area individually and not mean normalized, they contain the complete cytoarchitectonic information specific for the respective area (laminar cytoarchitectonic pattern, mean GLI, and relative width of cortical layers).

Borders between BAs 5 and 7 and Area hIP3

Common cytoarchitectonic features of BAs 5 and 7 were a gradual transition from layer II to layer III, a continuous increase (= gradient) of the volume fraction of pyramidal cells from upper to lower layer III, and a sublamination of layer V (Figs. 7 and 10–12). Both latter features were reflected as increases (layer III) or decreases (layer V), respectively, in the corresponding mean GLI profiles (Figs. 10–12: arrowheads). In upper layer Va, the volume fraction of the pyramidal cells was greater than in lower layer Vb (Fig. 7*B*: inset at bottom; Figs. 10–12: arrowheads). Hence, layer Vb appeared as a bright, sharply demarcated stripe, which separated layer Va from layer VI (Fig. 7*B*: inset at bottom; Figs. 10–12: arrowheads). The gradients within layers III and V, however, were stronger in BA 7 than in BA 5 (Fig. 7*A*: arrowheads; Figs. 10–12; see below) and differed also between their subareas (see below). A characteristic feature of BA 5 was the occurrence of interspersed "giant" pyramidal cells in layers Va and Vb, which exceeded the average size of the cells of this layer (Figs. 7*A* and 10: insets). The frequency of these cells differed between the subareas (see below).

The main features distinguishing hIP3 from BAs 5 and 7 were a sharper transition from layer II to layer III (Fig. 7*B*: arrowheads), a noncontinuous, abrupt increase of the volume fraction of cell bodies in lower layer III, and a non-sublaminated layer V (Fig. 7*B*: inset at bottom; Figs. 10–13: arrowheads; see below). The abrupt increase of the volume fraction in lower layer III caused upper layer III to appear brighter compared with lower

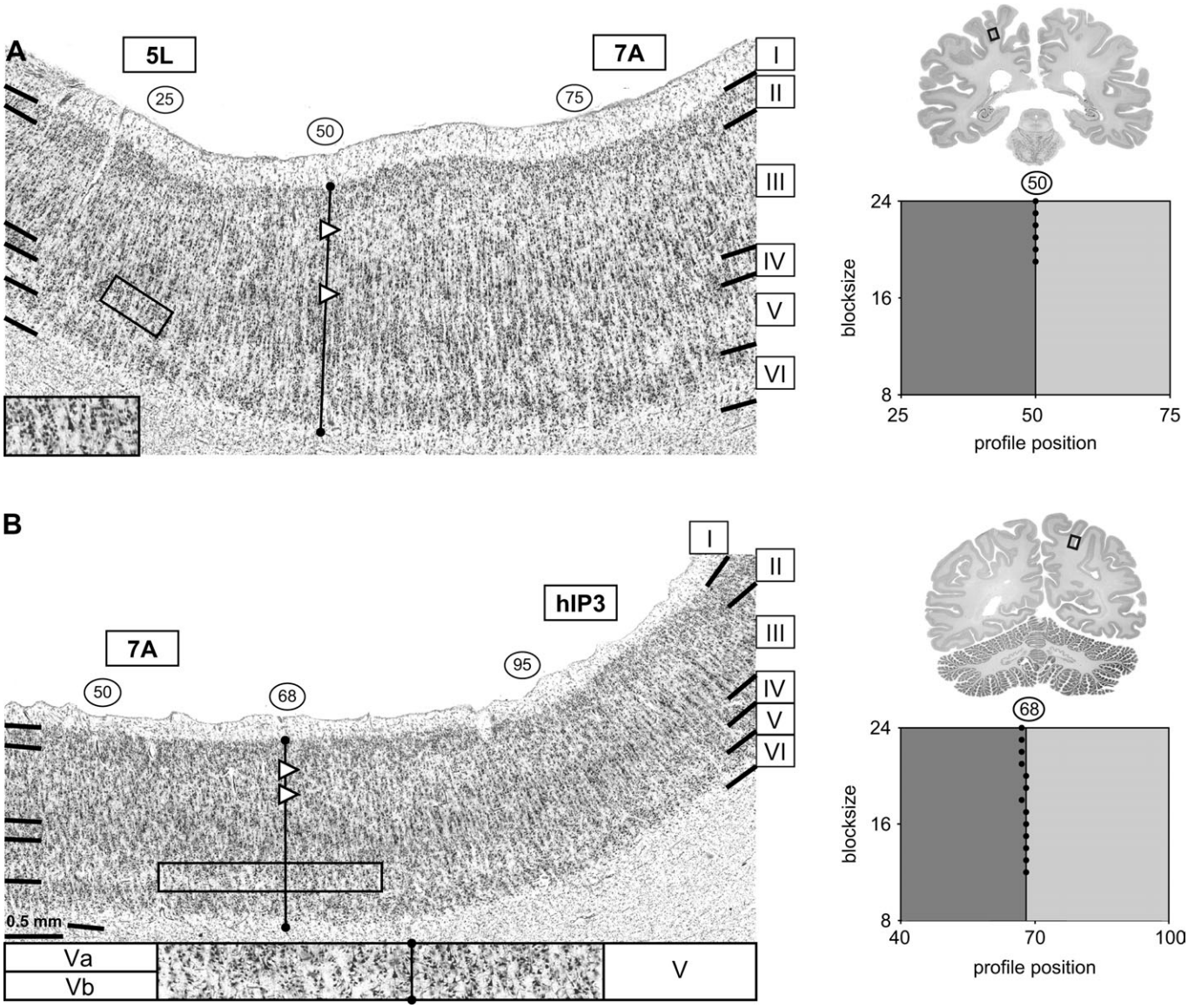

Figure 7. Cytoarchitectonic borders between (*A*) areas 5L and 7A (PoCS) and (*B*) areas 7A and hIP3 (IPS). Top right: cell-body–stained brain section with the marked location of the magnified region. Bottom right: plot indicating the location of significant maxima of the MD function (black dots) in the respective part of the ROI at different block sizes. Left: corresponding microphotograph rotated to show the cortical ribbon in an approximately horizontal orientation. The bar demarcates the profile position of the significant border. The insets show at 2-fold higher magnification (*A*) a giant pyramidal cell in layer V of area 5L and (*B*) layer V at the cytoarchitectonic border (bar) demonstrating the sublamination of layer V in area 7A, as compared with the more homogeneous appearance in area hIP3. Arrowheads point to (*A*) the stronger gradient of the volume fraction of cell bodies in layer III of BA 7 in comparison with BA 5 and (*B*) the brighter appearance of upper layer III and sharper transition between layers II and III in area hIP3 compared with BA 7.

layer III (Fig. 7*B*: arrowheads). Below the largest cells in lower layer III, which were arranged in a band-like fashion, a narrow stripe with a lower volume fraction of cell bodies was visible which separated these cells sharply from layer IV (Fig. 13: asterisks).

Borders of BAs 5 and 7 and Area hIP3 to Surrounding Areas

The characteristic feature of BAs 5 and 7 distinguishing them from the surrounding areas was the abovementioned prominent sublamination of layer V into 2 sublayers (Fig. 7*B*: inset at bottom; Fig. 8: asterisks; Figs. 10–12: arrowheads; Fig. 9).

Compared with postcentral BA 2, additional characteristics of BA 7 were a reduced volume fraction of cell bodies in upper layer III resulting in a stronger gradient in layer III and a sharper transition from layer II to layer III (Fig. 8*A*: arrowhead). An additional distinct feature in BA 5 were the giant pyramidal cells in layer V (Fig. 10: insets), which were absent in BA 2 (Fig. 8*A*).

The border of area 5Ci to the ventrally adjacent cingulate cortex was characterized by a decrease of the volume fraction of cell bodies in layers III and V in the latter region. At the border to the rostrally adjacent cingulate cortex layer IV disappeared. No giant pyramidal cells were found in layer V of the cingulate cortex. Compared with BA 7, the volume fraction of cell bodies in upper layer III was higher in the posterior cingulate cortex (pCi) leading to a reduced gradient in layer III and a more blurred transition between layers II and III (Fig. 8*B*: arrowhead). Lower layer III in pCi showed volume fractions that were comparable to (7A) or larger (7P and 7M) than those found in BA 7 (Figs. 8*B*, 11, and 12).

Several different areas with heterogenic cytoarchitecture abutting BA 7 were observed in the parieto-occipital sulcus

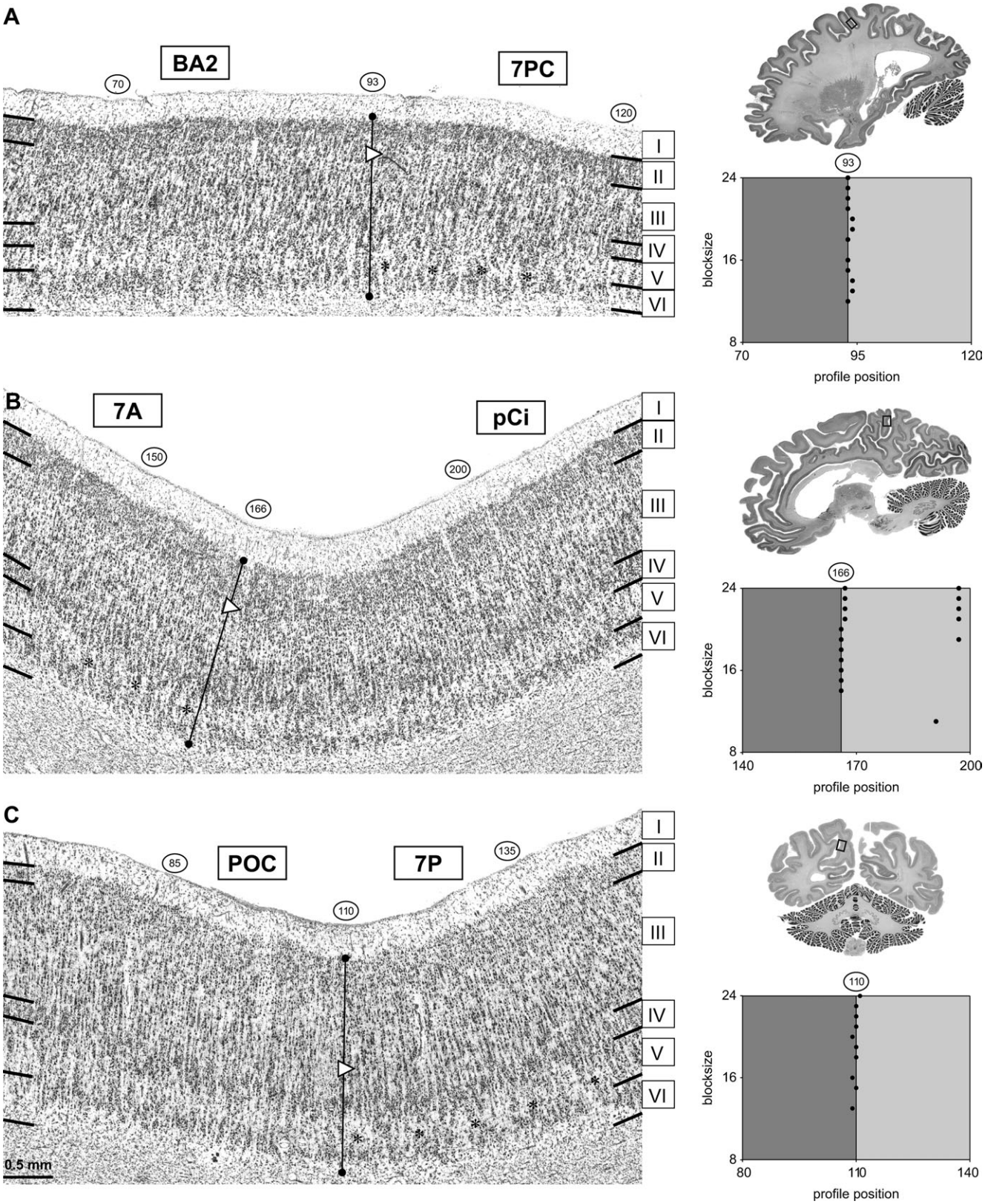

Figure 8. Cytoarchitectonic borders between (*A*) BA 2 and area 7PC (PoCS), (*B*) area 7A and the pCi (PrC), and (*C*) area 7P and the parieto-occipital cortex (POC; POS). Top right: cell-body–stained brain section with the marked location of the magnified region. Bottom right: plot indicating the location of significant maxima of the MD function (black dots) in the respective part of the ROI at different block sizes. Left: corresponding microphotograph rotated to show the cortical ribbon in an approximately horizontal orientation. The bar demarcates the profile position of the significant border. Asterisks indicate the bright appearance of layer Vb in BA 7 caused by a low volume fraction of cell bodies. Arrowheads point to (*A*) the lower volume fraction of cell bodies in upper layer III of area BA 7, resulting in a sharper transition between layers II and III and a stronger gradient in layer III compared with BA 2, (*B*) the higher volume fraction of cell bodies in upper layer III of pCi, resulting in a reduced gradient and a smoother transition to layer II in comparison with BA 7, and (*C*) the higher volume fraction of cell bodies in lower layer III of BA 7 and the resulting more pronounced gradient compared with the POC.

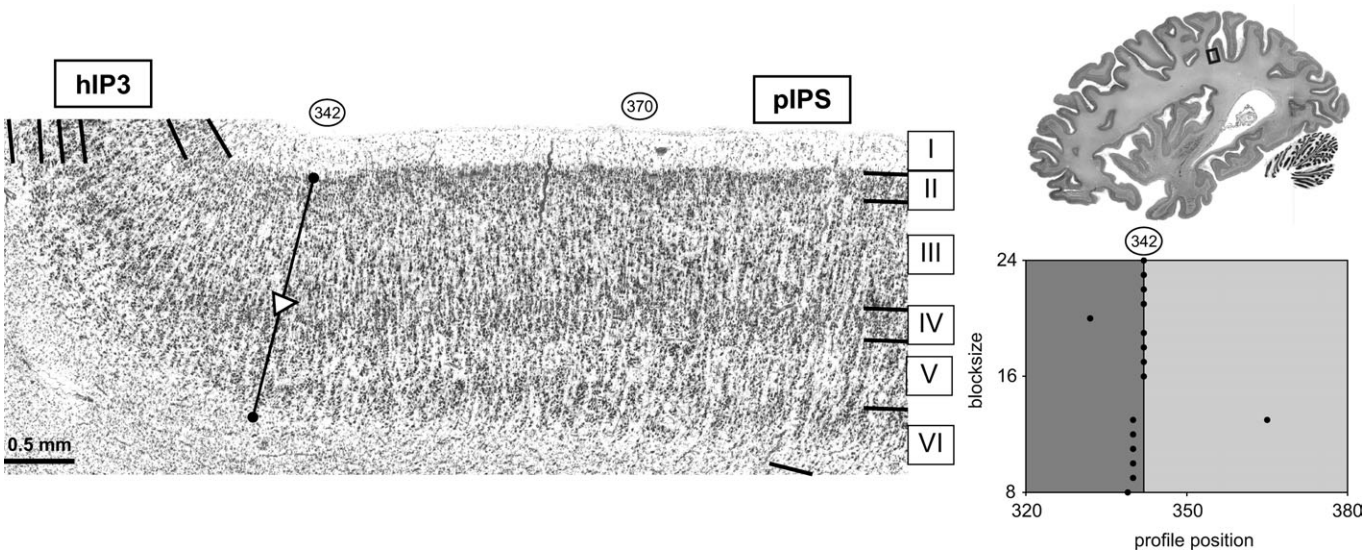

Figure 9. Cytoarchitectonic border between area hIP3 and the pIPS. Top right: cell-body–stained brain section with the marked location of the magnified region. Bottom right: Plot indicating the location of significant maxima of the MD function (black dots) in the respective part of the ROI at different block sizes. Left: corresponding microphotograph rotated to show the cortical ribbon in an approximately horizontal orientation. The bar demarcates the profile position of the significant border. The arrowhead indicates the transition from the band-like appearance of the pyramidal cells in lower layer III from area hIP3 to the more distributed pattern in pIPS.

(POS). These areas were not analyzed in detail in the context of the present study. Therefore, we only mention those criteria that were common to this "parieto-occipital cortex" (POC). The gradient in layer III of the POC was smaller than in BA 7, as was the volume fraction of cell bodies especially in lower layer III and layer V (Fig. 8*C*: arrowhead). Consequently, layer IV was better discernable in the POC.

Within the IPS, area hIP3 had borders with areas hIP1 and hIP2 laterally and with the posteriorly adjacent cortex in the medial wall of the IPS (pIPS). The borders to areas hIP1 and hIP2 were characterized by a more gradual and a less pronounced gradient in layer III of areas hIP1 and hIP2 (cf. Choi et al. 2006). The border between layers II and III was less clear in areas hIP1 and hIP2. Additionally, area hIP1 had a generally reduced volume fraction of cell bodies compared with area hIP3, whereas area hIP2 had a higher volume fraction and lacked the small stripe of very low volume fraction right above layer IV (Fig. 13: asterisks). Compared with area hIP3, the pIPS had a generally increased volume fraction of cell bodies (Fig. 9). In layer III of both areas, the gradient was strong and abrupt, but the largest pyramidal cells in the pIPS were not arranged in a band-like fashion like in hIP3 but were more vertically distributed (Fig. 9: arrowhead).

Subareas 5L, 5M, and 5Ci

In all subareas of BA 5, giant pyramidal cells were interspersed in layer V (Fig. 10: insets) with strong intersubject variability concerning size and frequency. These cells were less frequent and smaller in area 5L than in area 5M (Fig. 10: insets). Compared with area 5M, area 5L had smaller cells in layers III and V (Fig. 10). The sublamination of layer V was most pronounced in area 5L, corresponding to the GLI gradient within this layer in the mean profile (Fig. 10: arrowheads). In the upper part of layer VI, cells were arranged in a band-like fashion in areas 5M and 5Ci, whereas they were more distributed in area 5L. In layer III of area 5Ci, the volume fraction of cell bodies was reduced and showed a less pronounced gradient compared with area 5M (Fig. 10). At the border between areas 5M and 5Ci, layer IV became better discernable and the volume fraction of cell bodies in layer V increased toward area 5Ci. In area 5Ci, the frequency of giant pyramidal cells was the lowest within BA 5 (Fig. 10: insets), and the boundary to the white matter was sharper than in area 5M (Fig. 10).

Subareas 7PC, 7A, 7P, and 7M

Within BA 7, area 7PC showed a stronger gradient of the volume fraction of cell bodies in the superficial half of layer III in comparison with area 7A (Fig. 11). In lower layer III, the gradient was stronger in area 7A because the largest pyramidal cells in area 7PC were spaced further apart than in area 7A (Fig. 11). Of the 4 areas, 7A and 7P were most similar to each other. The cell size in layer III of area 7A was larger and the cell packing density lower than in area 7P (Figs. 11 and 12). Mostly due to the larger pyramidal cells in layer Va, the gradient of the volume fraction of cell bodies in layer V was stronger and the sublamination more prominent in area 7A than in area 7P (Figs. 11 and 12). In area 7M, the gradient in layer III was least pronounced and pyramidal cells in lower layer III were relatively small and more widely separated than in area 7P (Fig. 12).

Analysis of Cytoarchitecture Using GLI Profiles

Analysis of Laminar Cytoarchitectonic Patterns

For the analysis of laminar cytoarchitecture, normalized GLI profiles were PLWN corrected across areas to conform to one overall pattern of interlaminar borders (mean cortical depths: II/III 19%, III/IV 54%, IV/V 64%, and V/VI 79%).

Because the areas did not differ significantly between the hemispheres, mean profiles across both hemispheres were used for the MDS. The MDS arranged the points representing the mean GLI profiles across brains in a 2-dimensional space according to their degree of dissimilarity as measured by the

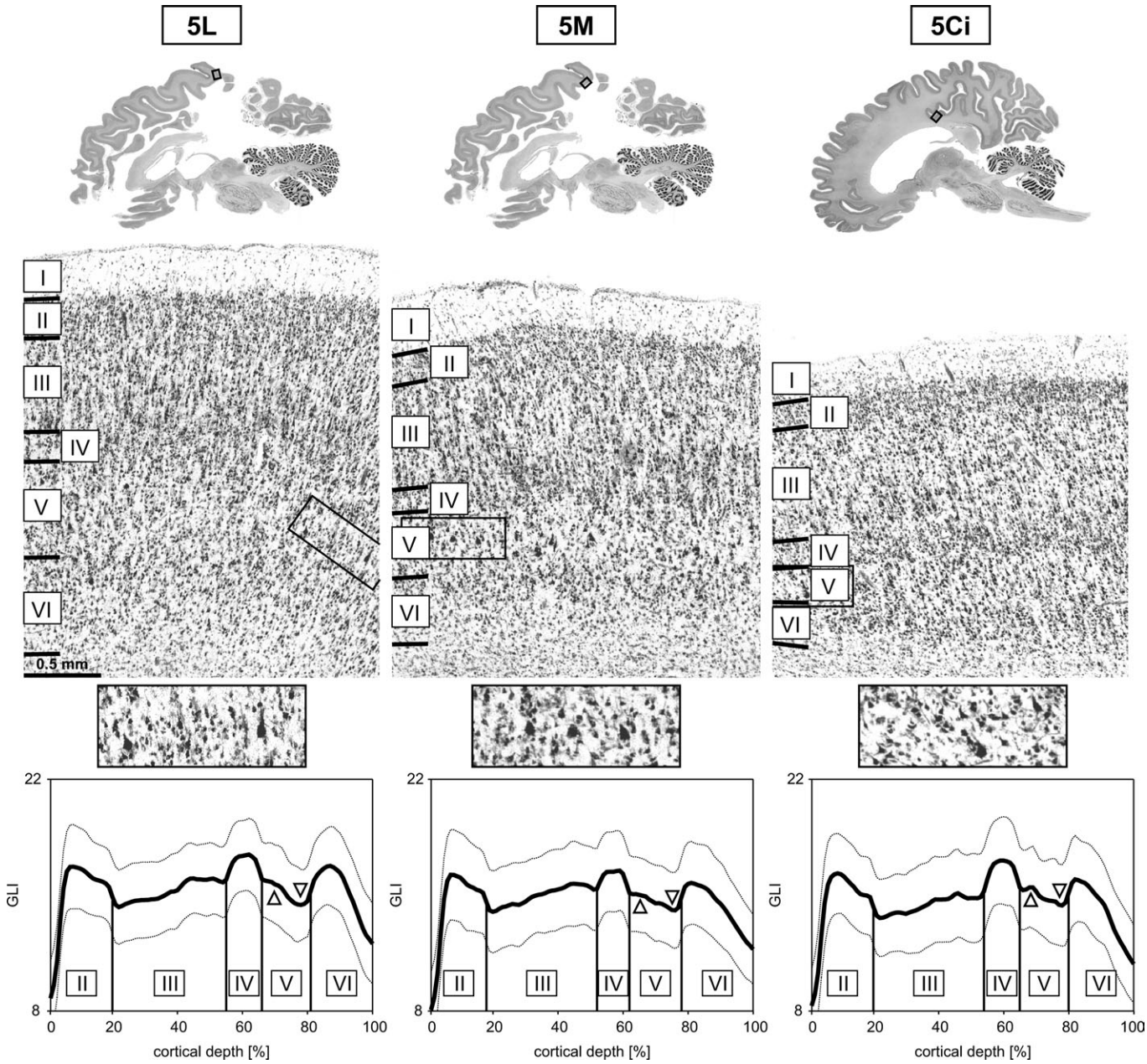

Figure 10. Cytoarchitecture of subareas within BA 5. Each column corresponds to one subarea. From top to bottom: cell-body–stained brain sections with the marked location of the respective rotated microphotograph shown below, insets showing the giant pyramidal cells in layer V at 2-fold higher magnification, and mean GLI profiles averaged across hemispheres and brains. Profiles are PLWN corrected separately for each area to reveal differences in laminar width. Dotted lines correspond to the standard deviation, and vertical lines demarcate the average cortical depths of the interlaminar borders for the respective area. Arrowheads indicate the representation of the sublamination of layer V in the GLI profile ($n = 10$).

ED (Fig. 14). High dissimilarity of 2 areas means that their points are far away from each other, and low dissimilarity means that they are close to each other. Each of the areas 5Ci, 5M, and hIP3 was separated from all other areas by relatively large distances, that is, their profile shapes had a high degree of dissimilarity to the shapes of the profiles of the remaining areas. The subareas of BA 7 were positioned relatively close to each other. The profiles of areas 7A and 7P were most similar, whereas areas 7PC and 7M had a higher degree of dissimilarity. Area 5L was positioned centrally between all other areas, but closer to the subareas of BA 7 than to those of BA 5. In the pairwise permutation tests between the areas, the profile of area 5Ci was significantly different from those of all other areas. The profile of area 5M was significantly different from those of all areas, except area 5L. The profile of area hIP3 was significantly different from those of all areas, except areas 5L and 7PC.

The specific differences between the profiles of the main areas 5 and 7 were visualized by subtracting a mean profile of subareas 5L and 5M from a mean profile of all subareas of BA 7. Area 5Ci was excluded because its profile differed significantly from those of areas 5L and 5M. The resulting difference profile is shown in Figure 15*A*. BA 7 had higher relative GLI values in layer IV, upper layer V, and layer VI, but lower values in layer II, upper layer III, and lower layer V. Consequently, the GLI increase

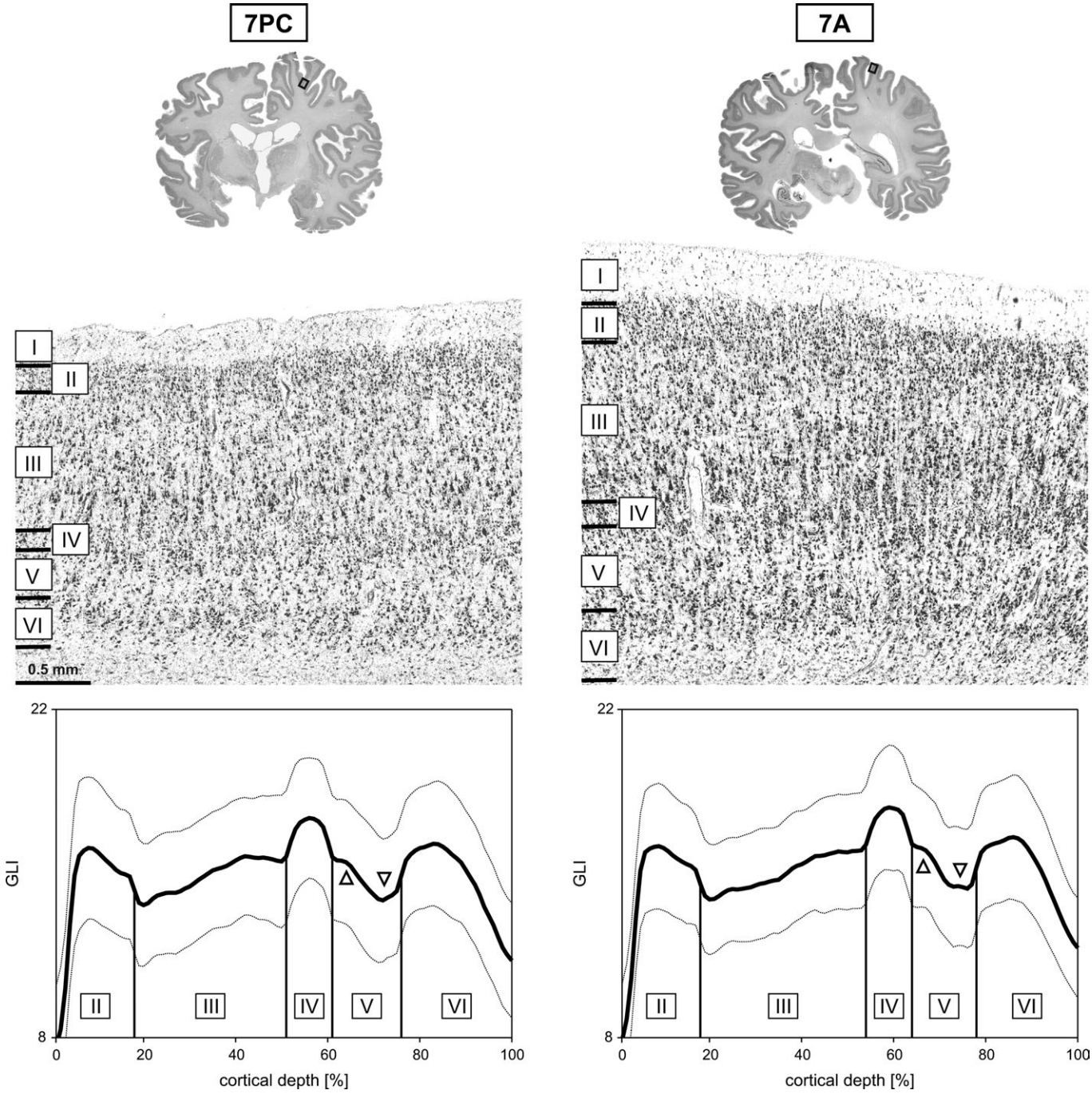

Figure 11. Cytoarchitecture of subareas within BA 7 (1). Each column corresponds to one subarea. From top to bottom: cell-body–stained brain sections with the marked location of the respective rotated microphotograph shown below and mean GLI profiles averaged across hemispheres and brains. Profiles are PLWN corrected separately for each area to reveal differences in laminar width. Dotted lines correspond to the standard deviation, and vertical lines demarcate the average cortical depths of the interlaminar borders for the respective area. Arrowheads indicate the representation of the sublamination of layer V in the GLI profile ($n = 10$).

within layer III and the GLI decrease within layer V were stronger in BA 7 than in areas 5L/M (Fig. 15*A*), corresponding to the abovementioned stronger gradients in BA 7 (Figs. 7*A* and 10–12).

The specific differences between the profiles of area hIP3 and BA 7 were visualized by subtracting a mean profile of all subareas of BA 7 from the mean profile of area hIP3. The difference profile is shown in Figure 15*B*. Area hIP3 had higher relative GLI values in layer II and a steeper GLI decrease toward layer III (Fig. 15*B*), corresponding to the sharper transition from layer II to layer III in the cytoarchitectonic picture (Fig. 7*B*: arrowheads). In upper and middle layer III, the values were similar in both areas. However, in lower layer III, the GLI values abruptly increased in hIP3 to higher relative values than in BA 7 (Fig. 15*B*). This corresponded to the sharply demarcated band of pyramidal cells in hIP3, in contrast to the continuous gradient in layer III of BA 7 (Figs. 11–13). In lower layer IV, the values in hIP3 were below those of BA 7. Compared with BA 7, the GLI in hIP3 was lower in upper layer V, but nearly equal in lower layer

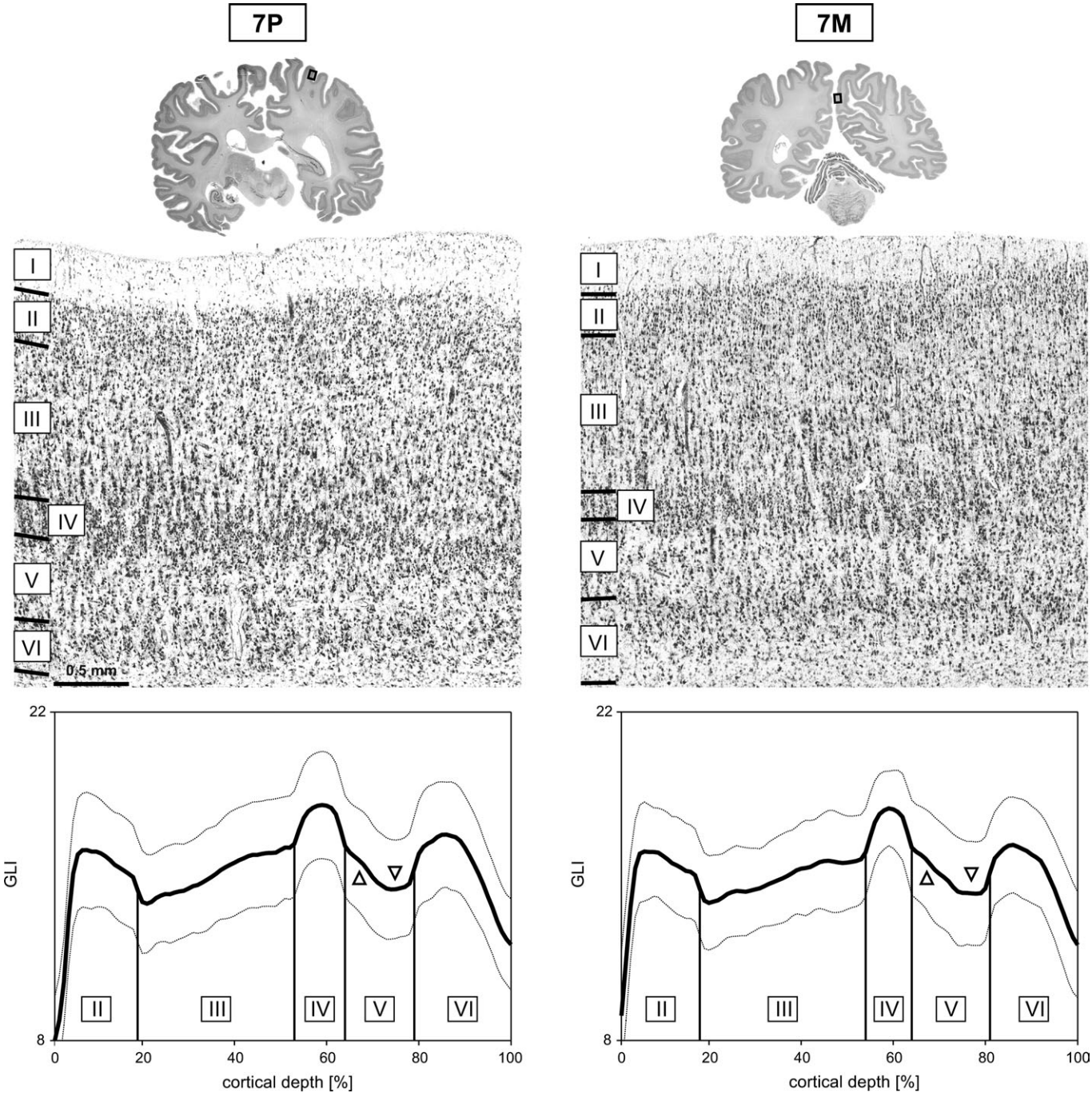

Figure 12. Cytoarchitecture of subareas within BA 7 (2). Each column corresponds to one subarea. From top to bottom: cell-body–stained brain sections with the marked location of the respective rotated microphotograph shown below and mean GLI profiles averaged across hemispheres and brains. Profiles are PLWN corrected separately for each area to reveal differences in laminar width. Dotted lines correspond to the standard deviation, and vertical lines demarcate the average cortical depths of the interlaminar borders for the respective area. Arrowheads indicate the representation of the sublamination of layer V in the GLI profile ($n = 10$).

V (Fig. 15*B*), which can be attributed to the sublamination of layer V in BA 7 which was not present in hIP3 (Fig. 7*B*: inset at bottom; Figs. 11–13: arrowheads). In upper layer VI, values were higher in area hIP3 and the GLI decrease toward the white matter steeper than in BA 7.

The specific differences between the profiles of subareas 5M and 5L are shown by the difference profile in Figure 15*C*. Area 5M had higher GLI values in layer III caused by the larger size and thus larger volume fraction of cells compared with area 5L (Fig. 10). Another difference in comparison with area 5L was the lower GLI in upper layer V compared with higher values in lower layer V of area 5M, corresponding to the less pronounced sublamination (Fig. 10: arrowheads). Finally, the GLI value began to decrease more superficially in layer VI of area 5M causing a negative slope in the difference profile and corresponding to the narrower band of cells in upper layer VI of area 5M (Fig. 10).

The specific differences between the profiles of subareas 5Ci and 5M were visible when the mean profile of area 5M was

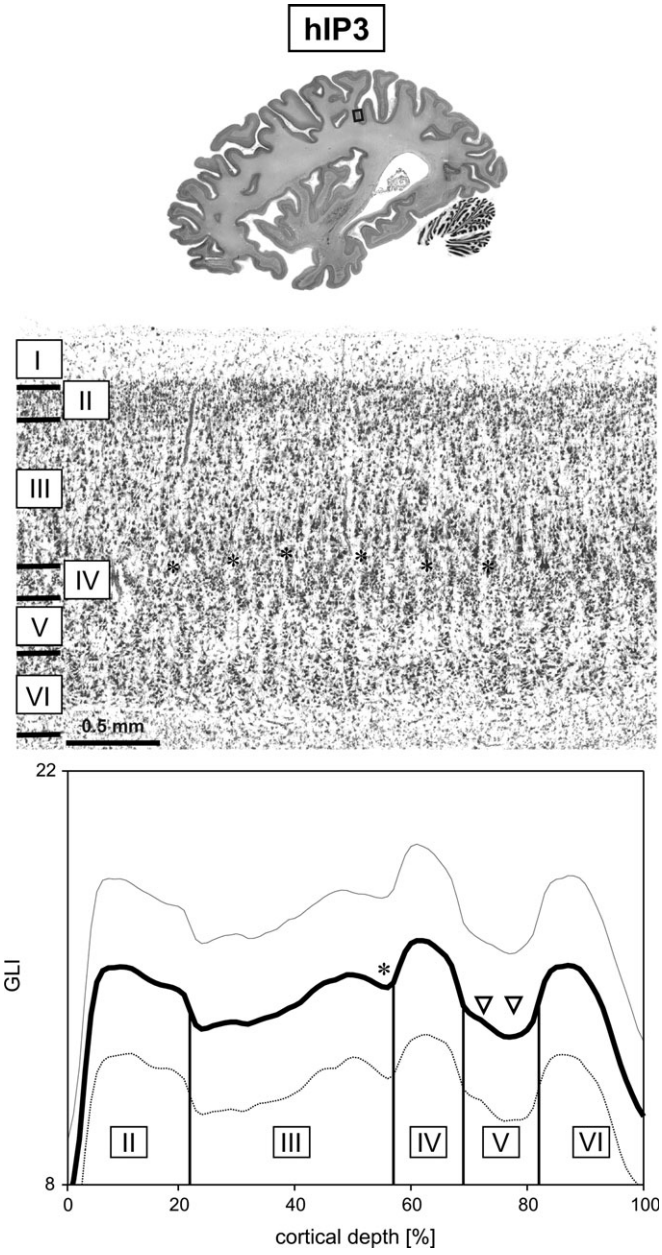

Figure 13. Cytoarchitecture of area hIP3. From top to bottom: cell-body–stained brain section with the marked location of the rotated microphotograph shown below and mean GLI profile averaged across hemispheres and brains. The profile is PLWN corrected separately for this area to reveal differences in laminar width. Dotted lines correspond to the standard deviation, and vertical lines demarcate the average cortical depths of the interlaminar borders. Asterisks indicate the bright narrow stripe above layer IV and its representation in the GLI profile. Arrowheads indicate the missing sublamination in layer V in the GLI profile ($n = 10$).

subtracted from that of area 5Ci (Fig. 15*D*). In layer III, the difference profile had a negative slope and showed lower values in lower layer III of area 5Ci, corresponding to the reduced volume fraction and gradient in the cytoarchitectonic picture (Fig. 10). At the border between layers III and IV, there was a sharp increase in the difference profile to higher relative GLI values in layers IV and V of area 5Ci, which reflected the sharper appearance of layer IV and the higher volume fraction of cell bodies (Fig. 10). In layer VI, the slope of the difference profile was negative representing the sharper transition to the white matter in area 5Ci (Fig. 10).

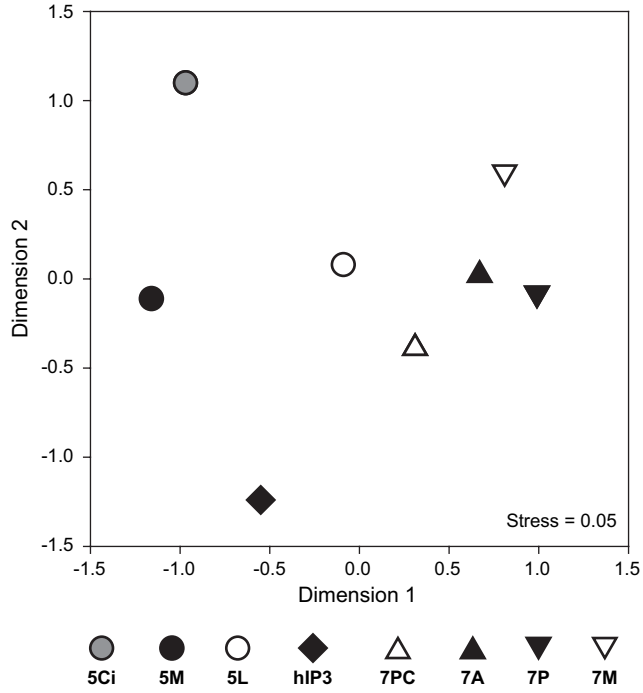

Figure 14. Scatter plot visualizing the results of the MDS for the mean GLI profiles of the areas across hemispheres and brains. Profiles were mean normalized and PLWN corrected across all areas and thus reflect laminar cytoarchitecture. MDS can be conceptualized as a rotation of the points representing the GLI profiles in 100-dimensional space that maximizes their apparent dispersion in a 2-dimensional subspace. This subspace is spanned by the 2 eigenvectors of the data matrix associated with the largest eigenvalues and, hence, brings the principal components of the data into view. The 2 principal components thus define the axes of the plot and the coordinate values for individual areas represent their respective component loads ($n = 10$).

The laminar cytoarchitectonic differences between neighboring subareas of BA 7 (Figs. 11 and 12) were reflected in their difference profiles (Fig. 15 *E–G*) although they were more subtle than those between the profiles of the subareas of BA 5 (Fig. 15 *C,D*). This was in correspondence with the results of the MDS (Fig. 14). Compared with the profile of area 7A, the profile of area 7PC had a stronger increase of the GLI in the superficial half of layer III (Fig. 15*E*), corresponding to the stronger gradient of the volume fraction of cell bodies in area 7PC (Fig. 11). In lower layer III, the slope of the difference profile was negative (Fig. 15*E*), reflecting the wider spacing of the pyramidal cells in area 7PC (Fig. 11). In layer III of areas 7A and 7P, the opposite differences of cell size and packing density (Figs. 11 and 12) resulted in nearly equal volume fractions of cell bodies, that is, GLI values (Fig. 15F). However, area 7A had higher relative GLI values in upper layer V and a stronger decrease toward lower layer V (Fig. 15*F*), corresponding to the more prominent sublamination in area 7A (Figs. 11 and 12). The difference profile of areas 7P and 7M had a positive slope in layer III (Fig. 15*G*), reflecting the stronger gradient in area 7P (Fig. 12).

Analysis of Differences in Mean GLI

None of the defined areas showed significant interhemispheric differences of the mean GLI ($P > 0.05$; Fig. 16). The ANOVA for interareal differences in mean GLI across both hemispheres revealed a significantly lower mean GLI in area hIP3 when contrasted with areas 5L, 7A, 7P, and 7M.

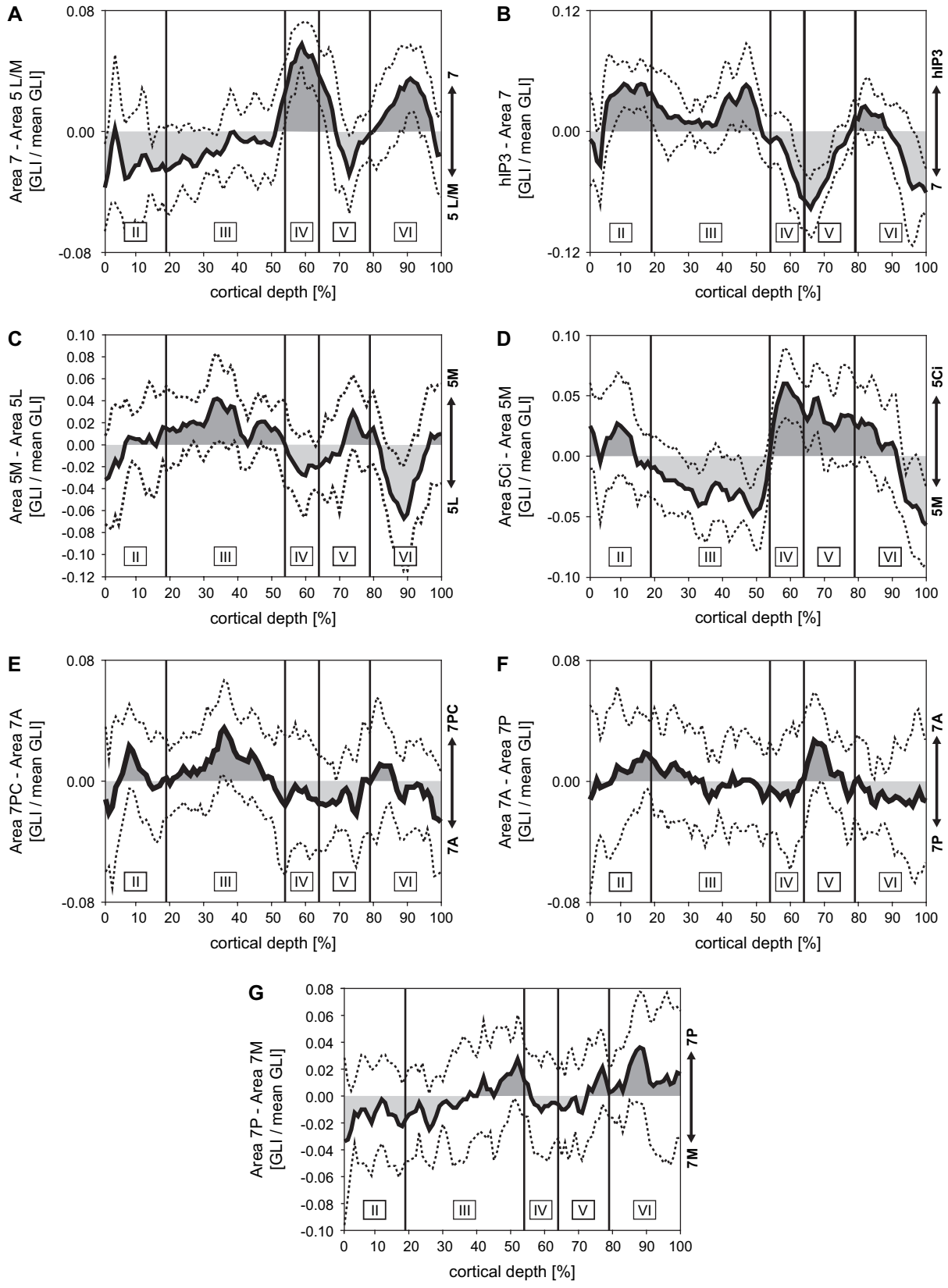

Figure 15. GLI difference profiles showing differences of laminar cytoarchitecture after mean normalization and PLWN correction across all areas. The respective areas that were compared are given on the right side of each graph. The profiles were calculated by subtracting the mean profile of the upper area from that of the lower area in each brain and subsequently averaging the difference profiles across brains. Higher relative GLI values in the upper or lower area, correspond to values above or below zero, respectively, and are emphasized by different gray shadings. Main areas: (*A*) areas 7PC, 7A, 7P, and 7M versus areas 5L and 5M; (*B*) area hIP3 versus areas 7PC, 7A, 7P, and 7M. Subareas of BA 5: (*C*) area 5M versus area 5L; (*D*) area 5Ci versus area 5M. Subareas of BA 7: (*E*) area 7PC versus area 7A; (*F*) area 7A versus area 7P; (*G*) area 7P versus area 7M. Dotted lines correspond to the standard deviation, and vertical lines demarcate the average cortical depths of the interlaminar borders (*A*, *B*, *G*: $n = 8$; *C*–*F*: $n = 10$).

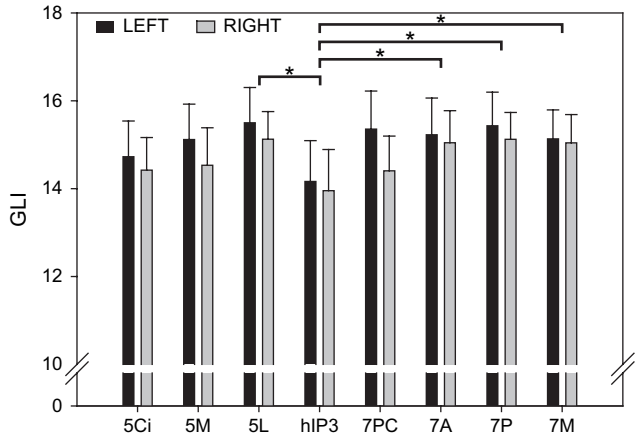

Figure 16. Bar graph showing for each area, the mean GLI values of the mean GLI profiles across brains for left and right hemispheres. Asterisks indicate pairs of areas that differed significantly by mean GLI of the mean GLI profiles across brains and hemispheres. (ANOVA; blocking factor: brain; $n = 10$; error bars = standard error of the mean).

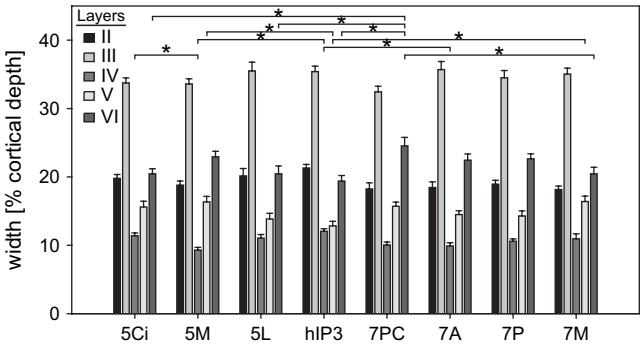

Figure 17. Bar graph showing for each area, the mean width of each cortical layer across hemispheres and brains. Asterisks indicate pairs of areas and layers that differed significantly. (ANOVA; blocking factor: brain; $n = 10$; error bars = standard error of the mean).

Analysis of Differences in the Relative Width of Cortical Layers

None of the areas and layers showed significant differences of the width between both hemispheres ($P > 0.05$; Fig. 17). The MANOVA for interareal differences using values averaged across hemispheres showed significant heterogeneity of laminar width in our sample ($P < 0.05$). The subsequent ANOVA revealed a significantly wider layer IV in area 5Ci in comparison with area 5M. Area hIP3 had a significantly wider layer IV than areas 5M and 7A and a significantly narrower layer V than areas 5M and 7M. Layer VI was significantly wider in area 7PC compared with areas 5Ci, 5L, 7M, and hIP3.

Topography of the Delineated Areas with Respect to Each Other and to Anatomical Landmarks

Values in parentheses indicate the percentage of the hemispheres in which the respective area/border was found at the respective location (number of hemispheres $n = 20$, if not indicated differently; Fig. 18).

Brodmann Area 5

1) Area 5L was found in the postcentral sulcus (PoCS) near to the interhemispheric fissure (PoCS: 100%; anterior wall: 75%; fundus: 90%; posterior wall: 85%). It was located medial and posterior to BA 2 (cf. Grefkes et al. 2001) and extended in about half of the hemispheres to the postcentral gyrus (60%) and in 90% to medial structures (cingulate sulcus [CiS]: 80%; PCL: 55%; PrC: 55%). In 95% of the hemispheres, it did not extend up to the IPS. In all left hemispheres, but only in half of the right hemispheres ($P < 0.05$), it extended posteriorly up to the anterior superficial part of the SPL (it was not possible to calculate an odds ratio for this difference because there was a 100%/0% ratio for left hemispheres). 2) Area 5M occupied parts (or the whole) of the superior/anterior wall of the posterior CiS (100%) and its ascending branch, extending to the posterior wall in about half of the hemispheres (45%). It reached to the PCL in 90% of the hemispheres and was located medial to area 5L and posterior/ventral to BA 4. In about half of the hemispheres, it extended into the medial branch of the central sulcus (60%) or to the lateral surface (55%). 3) Area 5Ci was located ventrally adjacent to area 5M in the superior wall of the CiS (100%), reaching to the inferior wall in 40% and to the PCL in half of the hemispheres. It extended further rostrally than area 5M and was ventrally and rostrally adjoined by the cingulate cortex (100%).

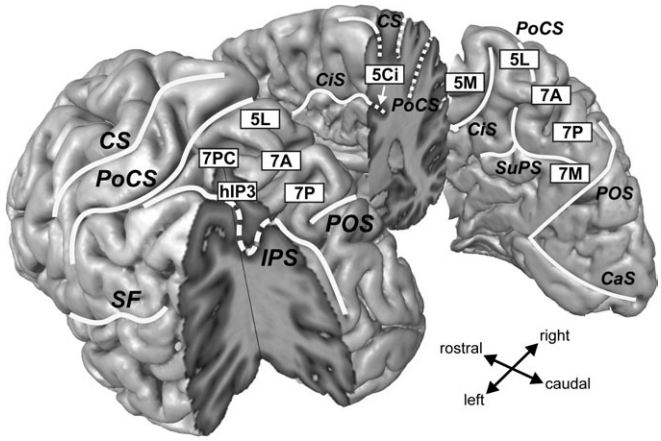

Figure 18. Schematic overview of the approximate locations of the cytoarchitectonic areas delineated in this study superimposed onto a 3-dimensional reconstruction of a human brain. The topography of areas on the lateral aspect is shown on the left hemisphere. A posterolateral segment of the left hemisphere is removed to allow the inspection of the depth and medial wall of the IPS. The topography of areas on the medial aspect is shown on the right hemisphere. The right hemisphere is coronally sectioned at the level of the central sulcus to allow the inspection of the walls of the CiS. White solid lines follow the superficial and dashed lines follow the deep course of the major sulci. CaS, calcarine sulcus; CS, central sulcus; SF, sylvian fissure.

Brodmann Area 7

1) Area 7PC was located on the lateral aspect of the anterior SPL (95%), posterior to BA 2 (cf. Grefkes et al. 2001), and lateral to area 5L. It occupied the posterior wall of the PoCS (95%) extending into the amIPS (90%). In 90% of the hemispheres it did not extend to the interhemispheric fissure. 2) Area 7A abutted areas 5L and 7PC posteriorly, occupying the largest part of the SPL (100%) and extending into the medial wall of the IPS (100%) and onto the PrC (95%). On the PrC, the dorsoventral location of the ventral border between area 7A and the cingulate cortex relative to the subparietal sulcus (SuPS) was variable (dorsal of SuPS: 95%; dorsal wall: 26%; fundus: 21%; ventral wall: 5%; ventral of SuPS: 5%; $n = 19$). 3) Area 7P was posteriorly adjacent to area 7A on the lateral and medial surface.

The location of the border between these 2 areas showed a high interindividual variability in the rostrocaudal dimension and was not demarcated reliably by any macroscopical landmark (e.g., SPL surface: 100%; superior parietal sulcus: anterior wall: 15%; fundus: 40%; and posterior wall: 50%). In only 20% of the left hemispheres, the border was located in the posterior wall of the superior parietal sulcus, whereas this was the case in 80% of the right hemispheres ($P < 0.05$; OR 16.0, 95% CI: 1.8–143.2). Laterally, area 7P extended to the IPS (70%) not as frequently as area 7A. Posteriorly, area 7P reached into the anterior wall of the POS in about half of the hemispheres (POS; 45%). Medially, it had borders with area 7M (94%; $n = 16$) and the cingulate cortex (80%). 4) Area 7M was located exclusively on the medial surface, posterior/ventral to area 7P. The border between these 2 areas varied in dorsoventral location with respect to the SuPS (dorsal of SuPS: 100%; dorsal wall: 33%; fundus: 53%; ventral wall: 20%; ventral of SuPS: 20%; $n = 15$). In 75% of the hemispheres, the posterior parts of area 7M extended into the anterior wall of the POS.

Area hIP3

Area hIP3 in the amIPS had borders with areas 7PC (90%) and 7A (85%). In most hemispheres, the anterior borders of area hIP3 were with area 7PC (amIPS: 94%; SPL surface: 50%; posterior wall of PoCS: 22%; $n = 18$), but occasionally, it extended into the fundus of the PoCS, adjoining BA 2 (36%; $n = 14$) or area 5L (25%). The locations of the borders with area 7A varied as well (IPS: medial wall: 100%; fundus: 18%; SPL surface: 35%; $n = 17$). Laterally, area hIP3 abutted areas hIP1 (IPS: medial wall: 43%; fundus: 86%, lateral wall: 43%; $n = 7$) or hIP2 (IPS: medial wall: 69%; fundus: 85%; lateral wall: 23%; $n = 13$; cf. Choi et al. 2006). Only in 10% of the hemispheres, area hIP3 extended posteriorly up to the level of area 7P.

Discussion

In the present study, 8 areas within the human SPC were delineated using observer-independent analysis of cytoarchitecture in 10 postmortem brains. This approach accounts for interindividual variability and makes differentiation even between cytoarchitectonic areas with minor differences reliable and reproducible. It represents a major advantage compared with previously published maps, which were based on the subjective visual analysis of brain sections from a very small sample or even only one single brain (Brodmann 1909, 1914; Vogt 1911; von Economo and Koskinas 1925; Gerhardt 1940; Sarkisov et al. 1955; Batsch 1956).

The algorithm detected borders between the areas consistently in all postmortem brains, although in the SPC, the cytoarchitecture showed a considerable interindividual variability, and interareal differences were more subtle than in some previously mapped cortical regions, primary areas in particular (Geyer et al. 1999; Amunts et al. 2000). Interindividual differences in parietal white matter anatomy have been associated with different levels of performance in visuospatial tasks (Tuch et al. 2005; Wolbers et al. 2006). It can hence be speculated that also interindividual differences in cortical cytoarchitecture might contribute to differences in behavioral performance (cf. Amunts et al. 2004).

Comparison with Previous Anatomical Descriptions

Structural segregations (Figs. 2 and 3) have been previously described in human SPC in terms of cytoarchitecture (Brodmann 1914; von Economo and Koskinas 1925; Gerhardt 1940; Sarkisov et al. 1955), myeloarchitecture (Vogt 1911; Batsch 1956), receptorarchitecture (Scheperjans, Grefkes, et al. 2005; Scheperjans, Palomero-Gallagher, et al. 2005), and connectivity (Rushworth et al. 2006).

The correspondence between our parcellation and those of previous authors is summarized in Table 1. Except for the pattern of areas in the mIPS (see below), the topographical extent of the areas in the SPC delineated in the present study was comparable to that reported in earlier publications (Figs. 2, 3, and 18; Brodmann 1909, 1914; Vogt 1911; von Economo and Koskinas 1925; Gerhardt 1940; Sarkisov et al. 1955; Batsch 1956; Geyer et al. 1996, 1999; Grefkes et al. 2001; Choi et al. 2006; Vogt et al. 2006). Previous maps differ mainly in the number of areas described within the SPC (Zilles et al. 2003; Table 1). Besides the abovementioned methodological factors, this may be attributed to the fact that the histological differences between the areas of the SPC and the surrounding cortex are relatively strong compared with those between the subareas within the SPC. Our map shows more subareas (Table 1; Figs. 2 and 18) than the maps of Brodmann (1909, 1914), von Economo and Koskinas (1925), and Sarkisov (1955). It resembles more the parcellation scheme suggested by Vogt (1911), Gerhardt (1940), and Batsch (1956), if only the main areas in these maps are considered (Table 1; Figs. 3 and 18). The extensive subparcellations of the main areas that were, for example, published by Gerhardt (1940), who delineated 34 subareas based on the analysis of one hemisphere, likely correspond to fluctuations of the cytoarchitectonic pattern within these areas. Such fluctuations might reflect topically organized functional spatial representations (Luppino et al. 1993; Fink et al. 1997; Sereno and Huang 2006) and were also observed in individual brains in the present study. However, no constant pattern emerged across the whole sample of brains that would be sufficient to derive additional subparcellations. This demonstrates that a sufficient sample size is needed in anatomical studies to separate genuine reproducible cytoarchitectonic differences between areas from individual cytoarchitectonic fluctuations.

The cytoarchitectonic descriptions of previous publications were mostly well reproducible in our study (Brodmann 1909; von Economo and Koskinas 1925; Gerhardt 1940; Grefkes et al. 2001; Scheperjans, Grefkes, et al. 2005; Scheperjans, Palomero-Gallagher, et al. 2005; Choi et al. 2006). The giant pyramidal cells in layer V (Fig. 10: insets) were previously mentioned as the main feature characterizing BA 5 (Brodmann 1909; von Economo and Koskinas 1925; Scheperjans, Grefkes, et al. 2005). Von Economo and Koskinas (1925) classified area PA_2 (i.e., BA 5; Table 1) as a subarea of area 3a of the primary somatosensory cortex. This, however, was neither confirmed in the present study nor by a recent observer-independent analysis of transmitter receptor distribution patterns, which suggested that BA 5 is clearly separated from area 3a and belongs to the parietal association cortex (Scheperjans, Grefkes, et al. 2005). Gerhardt (1940) noted that in area 75, which corresponds to BA 5 (Table 1), the giant pyramidal cells were not homogeneously distributed and not found in subarea 75scm in the CiS (Fig. 3). This is in line with our finding that these cells were rarely found in area 5Ci as compared with areas 5M and 5L (Fig. 10: insets). Our cytoarchitectonic subparcellation of BA 5 is further supported by a recent study showing distinct transmitter receptor distribution patterns in areas 5L, 5M, and 5Ci (Scheperjans, Grefkes, et al. 2005).

Von Economo and Koskinas (1925) noted a decrease of cell size within the region corresponding to BA 7 from rostral area PE_m to caudal area PE_p (Table 1; Fig. 2). This is confirmed by our finding of decreasing cell size from area 7A to area 7P (Figs. 11 and 12). However, we did not observe any equivalent of their most posterior subarea PE_γ with larger pyramidal cells compared with area PE_p. Rostrocaudal differences within BA 7 have also been described for transmitter receptor distribution patterns and linked to different functional properties of different subregions within this area (see below; Scheperjans, Palomero-Gallagher, et al. 2005). Comparison of the present parcellation with this recent receptorarchitectonic study suggests that the measuring sites 7PC, 7A, and 7P from that study had been placed in cytoarchitectonic areas 7PC, 7A, and 7P from the present study, respectively (Scheperjans, Palomero-Gallagher, et al. 2005). In the previous study, it was concluded that anatomical differences within BA 7 are more pronounced in the rostrocaudal than in the mediolateral dimension (Scheperjans, Palomero-Gallagher, et al. 2005). However, in the present study, area 7M was delineated ventrally on the PrC. Retrospectively, it can be assumed that this area was not included in the receptorarchitectonic study because data was obtained only from dorsal sites in the PrC near to the vertex. Consequently, we have to revise our previous statement (Scheperjans, Palomero-Gallagher, et al. 2005) in the sense that mediolateral anatomical differences exist in BA 7 at least in terms of cytoarchitecture.

In previous maps (Table 1; Fig. 2), the whole mIPS was often regarded as part of BA 2 (area PD; von Economo and Koskinas 1925) or BA 7 (Talairach and Tournoux 1988; Brodmann 1909). We cannot support this assumption because, in the present study, a new area (hIP3) was delineated in the amIPS, which was clearly distinct from BAs 5 or 7 in terms of cytoarchitecture (Figs. 7 and 10–17). We agree with Grefkes et al. (2001), who reported that BA 2 does not extend into the IPS and with Choi et al. (2006), who delineated distinct cytoarchitectonic areas (hIP1 and hIP2) in the lateral wall of the IPS.

Besides the abovementioned anatomical mapping techniques, immunohistochemistry is a powerful method to structurally parcellate the cerebral cortex. Most frequently applied in this context is the staining of a subset of corticocortically projecting pyramidal neurons, predominantly in lower layer III and upper layer V, using SMI-32 antibodies against nonphosphorylated neurofilaments (Campbell and Morrison 1989; Hof et al. 1995). With respect to a parcellation of the parietal cortex, to our knowledge, this method has so far been applied only for the brains of nonhuman primates (Hof and Morrison 1995; Lewis et al. 1999; Lewis and van Essen 2000; Luppino et al. 2005; Gregoriou et al. 2006). It seems to be more difficult to detect area-specific patterns in the human brain because of a greater proportion of immunoreactive neurons (Campbell and Morrison 1989). Evidence has been provided that cyto- and myeloarchitectonic borders between macaque superior parietal areas PE and PEc and the surrounding cortex (e.g., PEc/V6A, PE/cingulate cortex; Fig. 4) colocalize with changes in the size, shape, and distribution of SMI-32 immunoreactive pyramidal neurons (Hof and Morrison 1995; Lewis and van Essen 2000; Luppino et al. 2005). The border between macaque areas 2 and PE is more clearly visible in SMI-32 stainings than in cytoarchitectonic preparations (Lewis et al. 1999). Several borders between subareas of the SPC (e.g., PE/PEip, PE/MIP) can be seen in SMI-32 stained sections as well (Hof and Morrison 1995; Lewis and van Essen 2000). In the present study, 8 areas were reliably delineated based on cytoarchitectonic differences in the human SPC. Important distinctive features were the size and arrangement of pyramidal cells in layers III and V (Figs. 7–13 and 15). Therefore, immunohistochemical-selective staining of a subset of these cells with corticocortical connections using, for example, SMI-32 antibodies, may be useful in future studies to validate or extend the here presented parcellation. Furthermore, such data may be linked to connectivity patterns of the delineated areas as revealed by magnetic resonance imaging (Rushworth et al. 2006).

The analysis of the topographical relationships of the cytoarchitectonic areas revealed that, although the relative positions of the 8 areas were comparable between hemispheres and subjects, the locations of their borders with respect to macroanatomical landmarks showed strong interindividual variations. Therefore, the macroscopical structure of gyri and sulci cannot be used to predict the precise locations, sizes, or shapes of cytoarchitectonic areas in the SPC. This phenomenon has been noted previously with respect to other cortical regions (Geyer et al. 1996, 1999; Amunts et al. 1999; Grefkes et al. 2001; Morosan et al. 2001; Caspers et al. 2006; Choi et al. 2006; Eickhoff, Schleicher, et al. 2006; Malikovic et al. 2007; Rottschy et al. 2007) but is accounted for neither in historical brain atlases (Brodmann 1909, 1914; Vogt 1911; von Economo and Koskinas 1925; Gerhardt 1940; Sarkisov et al. 1955; Batsch 1956) nor in modern 3-dimensional adaptations of these maps (Talairach and Tournoux 1988). Probabilistic maps in stereotaxic space include information about intersubject variability and are the most suitable tools for the assignment of cortical activations to cytoarchitectonic areas in functional imaging studies (Amunts and Zilles 2001; Mazziotta et al. 2001; Zilles et al. 2002; Eickhoff et al. 2005; Uylings et al. 2005; Eickhoff, Heim, et al. 2006).

Analysis of GLI Profiles and Structural Relations between Areas

SPL, PrC, and PCL

Within BA 5, area 5Ci had the highest degree of dissimilarity to the remaining areas in terms of profile shape and laminar width (Figs. 10, 14, 15, 17). The GLI profiles of area 5L were more similar in shape to those of BA 7 than to those of areas 5M or 5Ci (Fig. 14). Areas 5L and 5Ci were nevertheless classified as parts of BA 5 because giant pyramidal cells, the characteristic feature of BA 5, were interspersed in layer V of both areas (Fig. 10: insets). Due to their only sporadic occurrence, these cells were not adequately represented in the GLI profiles. It has been recently described that transmitter receptor distribution patterns of areas 5L, 5M, and 5Ci are similar to those of area 7PC (Scheperjans, Palomero-Gallagher, et al. 2005). However, the patterns of area 5L are even more similar to those of postcentral somatosensory BA 2 and those of area 5Ci are more similar to those of the cingulate cortex (Scheperjans, Grefkes, et al. 2005; Scheperjans, Palomero-Gallagher, et al. 2005). Thus, the different subareas of BA 5 combine neurochemical and cytoarchitectonic features, which relate each of them differently to the surrounding postcentral, cingulate, and posterior parietal areas.

The borders between the subareas of BA 7 were detected as significant maxima of the MD function in the sections of the individual brains, although the cytoarchitectonic differences within BA 7 were more subtle than within BA 5 (Figs. 14 and 15). The analysis of GLI difference profiles revealed differences

between areas 7PC, 7A, 7P, and 7M (Fig. 15 *E–G*),which were, however, smaller than those between the main areas 5, 7, and hIP3 (Fig. 15 *A,B*), supporting our classification of these areas as subareas of BA 7. Possibly due to the strong interindividual cytoarchitectonic variability, the mean profiles of these 4 areas across brains did not differ significantly in the permutation tests. Cytoarchitectonic differences within BA 7 were strongest between areas 7PC and 7M and more subtle between areas 7A and 7P (Figs. 11, 12, 14, and 17). Additionally, the GLI profiles of area 7PC were similar in shape to those of area 5L (Fig. 14). However, layer VI was significantly wider in area 7PC (Fig. 17). In terms of receptor architecture, area 5L is closest related to the somatosensory cortex (BA 2; Scheperjans, Palomero-Gallagher, et al. 2005). Receptor distributions in area 7P are most similar to those of the extrastriate visual cortex. Areas 7PC and 7A show different degrees of anatomical similarity to adjacent areas, depending on the applied mapping technique (Scheperjans, Palomero-Gallagher, et al. 2005). Subtle cytoarchitectonic differences were found between areas 7A and 7P but no mediolateral differences within each area. This is in line with receptorarchitectonic observations where differences between areas 7A and 7P were stronger than between medial and lateral sites within each of these areas (Scheperjans, Palomero-Gallagher, et al. 2005).

In summary, the cytoarchitectonic analysis of the SPC in this study corroborated the results of previous receptorarchitectonic investigations concerning the subparcellation of BAs 5 and 7. However, it becomes clear that the measured degrees of architectonic similarity between cortical (sub)areas can differ depending on the mapping technique. This is not surprising because each method visualizes different structural correlates of physiological processes, which in concert are the basis for the specific functional properties of each cortical area.

Anterior Medial Wall of the IPS

Area hIP3 in the amIPS was clearly distinct from the other delineated areas in terms of laminar pattern and mean GLI (Figs. 7 and 10–17). In this area, layer IV had a larger and layers V and VI a smaller relative width compared with several other areas (Fig. 17). This is probably reflecting the influence of cortical folding on laminar width because profiles of area hIP3 were nearly exclusively sampled from the depth of the IPS, whereas those of the other areas (5M, 7PC, 7A, and 7M) were more often sampled from the free cortical surface (generally, deep cortical layers tend to be relatively narrower and superficial layers relatively wider in sulci than at the crowns of gyri; von Economo and Koskinas 1925; Bok and von Kip 1936; Eickhoff et al. 2007). Concerning the significantly wider layer IV and narrower layer VI in area 5Ci compared with areas 5M and 7PC, respectively, a similar effect may play a role (Figs. 10, 11, and 17). This is less likely with respect to the differences between area 7PC and areas 5L and 7M (Figs. 10–12 and 17).

Comparison of Structural and Functional Data from Human and Macaque SPC

The pattern of areas in the human SPC that was revealed in the present study resembles the commonly assumed areal configuration of the macaque SPC (Figs. 4 and 18; Pandya and Seltzer 1982). The macaque SPC shows a rostrocaudal parcellation into areas PE and PEc on the lateral and mediodorsal surface resembling the rostrocaudal arrangement of areas 5L, 5M, and 7PC (rostral) and areas 7A and 7P (caudal). In line with these structural findings, regionally different functional properties have been described within the SPC of both species, for example, gradients of the relative functional influences of the somatosensory (anterior SPL) and visual (posterior SPL) modalities (Mountcastle et al. 1975; Squatrito et al. 2001; Stoeckel et al. 2004; Breveglieri et al. 2006; Wenderoth et al. 2006). This rostrocaudal functional scheme is structurally reflected in terms of neurotransmitter receptor distributions which show similar patterns in the anterior SPC (particularly area 5L) and somatosensory cortex, whereas the patterns in the posterior SPC (particularly area 7P) resemble those of extrastriate visual areas (Scheperjans, Palomero-Gallagher, et al. 2005).

The human posterior PCL (i.e., anterior medial SPC; BA 5) can be activated by somatosensory stimulation if subjects attend to the stimuli and electrostimulation of this region can elicit motor responses (Richer et al. 1993; Lim et al. 1994; Allison et al. 1996; Forss et al. 1996). Additionally, the PCL plays an important role for the cerebral control of micturition (Sakakibara et al. 1999). In the CiS of the macaque, a higher order sensorimotor area (PEci) has been described at a location comparable to that of human area 5Ci (Figs. 4 and 18; Murray and Coulter 1981; Pandya and Seltzer 1982; Shima et al. 1991; Lacquaniti et al. 1995; Morecraft et al. 2004).

In humans and macaques, neural activity in the SPL, PrC, and the mIPS, which are sometimes referred to as parts of the parietal reach region (PRR), is functionally associated with somatosensory and visuomotor integration, particularly related to reaching movements, as well as visuospatial attentional and memory processes (Grèzes and Decety 2001; Battaglia-Mayer and Caminiti 2002; Buneo et al. 2002; Connolly et al. 2003; Rizzolatti and Matelli 2003; Cavanna and Trimble 2006; Culham et al. 2006; Curtis 2006; Hahn et al. 2006; Iacoboni 2006; Pellijeff et al. 2006; Ricciardi et al. 2006). Activation patterns in the SPL/IPS during visually guided reaching differ, however, depending on whether the target is presented in the center (mIPS) or the periphery (additionally posterior SPL) of the visual field (Prado et al. 2005). Also attentional processes involve separate parts of the SPC and IPS differently (Molenberghs et al. 2007). Besides its abovementioned properties, the PrC is one of the so-called cortical midline structures which are related to self-referential processing and are implicated in the "default mode" of brain function (Raichle et al. 2001; Cavanna and Trimble 2006; Northoff et al. 2006). In the present study, 3 areas (7A, 7P, and 7M) were delineated on the PrC, which might correspond to previously described functional segregations in this region (Cavanna and Trimble 2006). In macaques, the ventral part of the PrC is occupied by area PGm (Fig. 4; Pandya and Seltzer 1982). It could be speculated that this area corresponds to human area 7M.

In the human and macaque IPS, several distinct regions have been anatomically and functionally characterized (Fig. 4; Lewis and van Essen 2000; Grefkes et al. 2004; Grefkes and Fink 2005; Choi et al. 2006; Culham et al. 2006; Iacoboni 2006; Orban et al. 2006; Rushworth et al. 2006). Because the human IPS has a much more complex structure than the macaque IPS, direct structural comparisons of this region between species are difficult (Choi et al. 2006). In the macaque mIPS (Fig. 4; Matelli et al. 1998; Grefkes and Fink 2005), the most commonly described areas are PEip (anterior) and MIP (posterior). Several functionally distinct areas have also been identified in the

human (e.g., dorsal IPS anterior [DIPSA], dorsal IPS medial [DIPSM], the human MIP equivalent [hMIP]); however, no generally accepted parcellation exists (Grefkes et al. 2004; Grefkes and Fink 2005; Culham et al. 2006; Iacoboni 2006; Orban et al. 2006). The present study is the first to provide evidence for a distinct cytoarchitectonic area (hIP3) in the amIPS.

It seems reasonable to assume that the here described subareas of BAs 5 and 7, as well as area hIP3, are the structural correlates of functional segregations within the human SPC.

Interhemispheric Differences

Statistically confirmed interhemispheric differences in cytoarchitecture have been described for several cortical areas based on sample sizes comparable to that of the present study (e.g., primary motor cortex and Broca's area; Amunts et al. 1996, 2003; Uylings et al. 2006). Reports about structural asymmetries of superior parietal gray matter are inconsistent (Good et al. 2001; Watkins et al. 2001; Luders et al. 2006). In the functional domain, rightward lateralization has been described within parietal cortex for attentional processes (Culham et al. 2006). However, many tasks involving reaching showed contra- or bilateral activations (Culham et al. 2006). In the present study, we found no evidence for interhemispheric differences of area-specific cytoarchitecture in the SPC. Any confounding effect of differential cortical thickness between hemispheres was excluded because the length of every GLI profile was normalized for subsequent analyses. However, on the macroscopical level, the topography of 3 cytoarchitectonic areas and their borders (5L, 7A, and 7P) in relation to anatomical landmarks showed significant interhemispheric differences, which may be functionally relevant. In addition to the analysis of white matter pathways (Barrick et al. 2007), volumetric analyses of cytoarchitectonically defined cortical areas may be useful in the future for the detection of anatomical correlates of hemispheric functional specialization in the SPC.

We plan to present in the near future probabilistic maps in stereotaxic space (Amunts and Zilles 2001; Mazziotta et al. 2001) and volumetric analyses of the areas delineated in the present study. This may reveal additional anatomical substrates of functional differences between, for example, hemispheres or genders. Furthermore, the maps will enable investigators to directly correlate activations obtained from functional imaging experiments with observer-independently acquired cytoarchitectonic information to explore structure-function relationships within the SPC (Eickhoff et al. 2005; Eickhoff, Heim, et al. 2006).

Funding

Deutsche Forschungsgemeinschaft (KFO 112); The National Institute of Biomedical Imaging and Bioengineering, The National Institute of Neurological Disorders and Stroke, and The National Institute of Mental Health (Human Brain Project/Neuroinformatics Research grant); European Commission (QLG3-CT-2002-00746); Helmholtz Gemeinschaft.

Notes

The authors thank U. Blohm and F. Kocaer for excellent histological work and for assistance with image acquisition. *Conflict of Interest*: None declared.

Address correspondence to email: filip@gmx.net.

References

Allison T, McCarthy G, Luby M, Puce A, Spencer DD. 1996. Localization of functional regions of human mesial cortex by somatosensory evoked potential recording and by cortical stimulation. Electroencephalogr Clin Neurophysiol. 100:126–140.

Amunts K, Istomin V, Schleicher A, Zilles K. 1995. Postnatal development of the human primary motor cortex: a quantitative cytoarchitectonic analysis. Anat Embryol (Berl). 192:557–571.

Amunts K, Malikovic A, Mohlberg H, Schormann T, Zilles K. 2000. Brodmann's areas 17 and 18 brought into stereotaxic space-where and how variable? Neuroimage. 11:66–84.

Amunts K, Schlaug G, Schleicher A, Steinmetz H, Dabringhaus A, Roland PE, Zilles K. 1996. Asymmetry in the human motor cortex and handedness. Neuroimage. 4:216–222.

Amunts K, Schleicher A, Burgel U, Mohlberg H, Uylings HB, Zilles K. 1999. Broca's region revisited: cytoarchitecture and intersubject variability. J Comp Neurol. 412:319–341.

Amunts K, Schleicher A, Ditterich A, Zilles K. 2003. Broca's region: cytoarchitectonic asymmetry and developmental changes. J Comp Neurol. 465:72–89.

Amunts K, Schleicher A, Zilles K. 2004. Outstanding language competence and cytoarchitecture in Broca's speech region. Brain Lang. 89:346–353.

Amunts K, Zilles K. 2001. Advances in cytoarchitectonic mapping of the human cerebral cortex. Neuroimaging Clin N Am. 11:151–69, vii.

Barrick TR, Lawes IN, Mackay CE, Clark CA. 2007. White matter pathway asymmetry underlies functional lateralization. Cereb Cortex. 17:591–598.

Batsch EG. 1956. Die myeloarchitektonische Untergliederung des Isocortex parietalis beim Menschen. J Hirnforsch. 2:225–258.

Battaglia-Mayer A, Caminiti R. 2002. Optic ataxia as a result of the breakdown of the global tuning fields of parietal neurones. Brain. 125:225–237.

Bok ST, von Kip M. 1936. The size of the body and the size and the number of the nerve cells in the cerebral cortex. Acta Ned Morphol. 3:1–22.

Breveglieri R, Galletti C, Gamberini M, Passarelli L, Fattori P. 2006. Somatosensory cells in area PEc of macaque posterior parietal cortex. J Neurosci. 26:3679–3684.

Brodmann K. 1909. Vergleichende Lokalisationslehre der Großhirnrinde—in ihren Prinzipien dargestellt auf Grund des Zellenbaues. Leipzig (Germany): Verlag von Johann Ambrosius Barth.

Brodmann K. 1914. Physiologie des Gehirns. In: Knoblauch A, Brodmann K, Hauptmann A, editors. Die allgemeine Chirurgie der Gehirnkrankheiten. Stuttgart (Germany): Verlag von Ferdinand Enke. p. 397.

Buneo CA, Jarvis MR, Batista AP, Andersen RA. 2002. Direct visuomotor transformations for reaching. Nature. 416:632–636.

Campbell MJ, Morrison JH. 1989. Monoclonal antibody to neurofilament protein (SMI-32) labels a subpopulation of pyramidal neurons in the human and monkey neocortex. J Comp Neurol. 282:191–205.

Caspers S, Geyer S, Schleicher A, Mohlberg H, Amunts K, Zilles K. 2006. The human inferior parietal cortex: cytoarchitectonic parcellation and interindividual variability. Neuroimage. 33:430–448.

Cavanna AE, Trimble MR. 2006. The precuneus: a review of its functional anatomy and behavioural correlates. Brain. 129:564–583.

Choi HJ, Zilles K, Mohlberg H, Schleicher A, Fink GR, Armstrong E, Amunts K. 2006. Cytoarchitectonic identification and probabilistic mapping of two distinct areas within the anterior ventral bank of the human intraparietal sulcus. J Comp Neurol. 495:53–69.

Connolly JD, Andersen RA, Goodale MA. 2003. FMRI evidence for a 'parietal reach region' in the human brain. Exp Brain Res. 153:140–145.

Culham JC, Cavina-Pratesi C, Singhal A. 2006. The role of parietal cortex in visuomotor control: what have we learned from neuroimaging? Neuropsychologia. 44:2668–2684.

Curtis CE. 2006. Prefrontal and parietal contributions to spatial working memory. Neuroscience. 139:173–180.

Eickhoff SB, Heim S, Zilles K, Amunts K. 2006. Testing anatomically specified hypotheses in functional imaging using cytoarchitectonic maps. Neuroimage. 32:570–582.

Eickhoff SB, Schleicher A, Scheperjans F, Palomero-Gallagher N, Zilles K. 2007. Analysis of neurotransmitter receptor distribution patterns in the cerebral cortex. Neuroimage. 34:1317–1330.
Eickhoff SB, Schleicher A, Zilles K, Amunts K. 2006. The human parietal operculum. I. Cytoarchitectonic mapping of subdivisions. Cereb Cortex. 16:254–267.
Eickhoff SB, Stephan KE, Mohlberg H, Grefkes C, Fink GR, Amunts K, Zilles K. 2005. A new SPM toolbox for combining probabilistic cytoarchitectonic maps and functional imaging data. Neuroimage. 25:1325–1335.
Fink GR, Frackowiak RS, Pietrzyk U, Passingham RE. 1997. Multiple nonprimary motor areas in the human cortex. J Neurophysiol. 77:2164–2174.
Forss N, Merlet I, Vanni S, Hamalainen M, Mauguiere F, Hari R. 1996. Activation of human mesial cortex during somatosensory target detection task. Brain Res. 734:229–235.
Gerhardt E. 1940. Die Cytoarchitektonik des Isocortex parietalis beim Menschen. J Psychol Neurol. 40:367–419.
Geyer S, Ledberg A, Schleicher A, Kinomura S, Schormann T, Burgel U, Klingberg T, Larsson J, Zilles K, Roland PE. 1996. Two different areas within the primary motor cortex of man. Nature. 382:805–807.
Geyer S, Schleicher A, Zilles K. 1999. Areas 3a, 3b, and 1 of human primary somatosensory cortex. Neuroimage. 10:63–83.
Good CD, Johnsrude I, Ashburner J, Henson RN, Friston KJ, Frackowiak RS. 2001. Cerebral asymmetry and the effects of sex and handedness on brain structure: a voxel-based morphometric analysis of 465 normal adult human brains. Neuroimage. 14:685–700.
Grefkes C, Fink GR. 2005. The functional organization of the intraparietal sulcus in humans and monkeys. J Anat. 207:3–17.
Grefkes C, Geyer S, Schormann T, Roland P, Zilles K. 2001. Human somatosensory area 2: observer-independent cytoarchitectonic mapping, interindividual variability, and population map. Neuroimage. 14:617–631.
Grefkes C, Ritzl A, Zilles K, Fink GR. 2004. Human medial intraparietal cortex subserves visuomotor coordinate transformation. Neuroimage. 23:1494–1506.
Grefkes C, Weiss PH, Zilles K, Fink GR. 2002. Crossmodal processing of object features in human anterior intraparietal cortex: an fMRI study implies equivalencies between humans and monkeys. Neuron. 35:173–184.
Gregoriou GG, Borra E, Matelli M, Luppino G. 2006. Architectonic organization of the inferior parietal convexity of the macaque monkey. J Comp Neurol. 496:422–451.
Grèzes J, Decety J. 2001. Functional anatomy of execution, mental simulation, observation, and verb generation of actions: a meta-analysis. Hum Brain Mapp. 12:1–19.
Hahn B, Ross TJ, Stein EA. 2006. Neuroanatomical dissociation between bottom-up and top-down processes of visuospatial selective attention. Neuroimage. 32:842–853.
Hof PR, Morrison JH. 1995. Neurofilament protein defines regional patterns of cortical organization in the macaque monkey visual system: a quantitative immunohistochemical analysis. J Comp Neurol. 352:161–186.
Hof PR, Nimchinsky EA, Morrison JH. 1995. Neurochemical phenotype of corticocortical connections in the macaque monkey: quantitative analysis of a subset of neurofilament protein-immunoreactive projection neurons in frontal, parietal, temporal, and cingulate cortices. J Comp Neurol. 362:109–133.
Iacoboni M. 2006. Visuo-motor integration and control in the human posterior parietal cortex: evidence from TMS and fMRI. Neuropsychologia. 44:2691–2699.
Jones SE, Buchbinder BR, Aharon I. 2000. Three-dimensional mapping of cortical thickness using Laplace's equation. Hum Brain Mapp. 11:12–32.
Lacquaniti F, Guigon E, Bianchi L, Ferraina S, Caminiti R. 1995. Representing spatial information for limb movement: role of area 5 in the monkey. Cereb Cortex. 5:391–409.
Lewis JW, Burton H, van Essen DC. 1999. Anatomical evidence for the posterior boundary of area 2 in the macaque monkey. Somatosens Mot Res. 16:382–390.
Lewis JW, van Essen DC. 2000. Corticocortical connections of visual, sensorimotor, and multimodal processing areas in the parietal lobe of the macaque monkey. J Comp Neurol. 428:112–137.
Lim SH, Dinner DS, Pillay PK, Luders H, Morris HH, Klem G, Wyllie E, Awad IA. 1994. Functional anatomy of the human supplementary sensorimotor area: results of extraoperative electrical stimulation. Electroencephalogr Clin Neurophysiol. 91:179–193.
Luders E, Narr KL, Thompson PM, Rex DE, Jancke L, Toga AW. 2006. Hemispheric asymmetries in cortical thickness. Cereb Cortex. 16:1232–1238.
Luppino G, Hamed SB, Gamberini M, Matelli M, Galletti C. 2005. Occipital (V6) and parietal (V6A) areas in the anterior wall of the parieto-occipital sulcus of the macaque: a cytoarchitectonic study. Eur J Neurosci. 21:3056–3076.
Luppino G, Matelli M, Camarda R, Rizzolatti G. 1993. Corticocortical connections of area F3 (SMA-proper) and area F6 (pre- SMA) in the macaque monkey. J Comp Neurol. 338:114–140.
Mahalanobis PC, Majumda DN, Rao CR. 1949. Anthropometric survey of the united provinces. A statistical study. Sankhya. 9:89–324.
Malikovic A, Amunts K, Schleicher A, Mohlberg H, Eickhoff SB, Wilms M, Palomero-Gallagher N, Armstrong E, Zilles K. 2007. Cytoarchitectonic analysis of the human extrastriate cortex in the region of V5/MT+: a probabilistic, stereotaxic map of area hOc5. Cereb Cortex. 17:562–574.
Matelli M, Govoni P, Galletti C, Kutz DF, Luppino G. 1998. Superior area 6 afferents from the superior parietal lobule in the macaque monkey. J Comp Neurol. 402:327–352.
Mazziotta J, Toga A, Evans A, Fox P, Lancaster J, Zilles K, Woods R, Paus T, Simpson G, Pike B, et al. 2001. A probabilistic atlas and reference system for the human brain: International Consortium for Brain Mapping (ICBM). Phil Trans R Soc B. 356:1293–1322.
Merker B. 1983. Silver staining of cell bodies by means of physical development. J Neurosci Methods. 9:235–241.
Molenberghs P, Mesulam MM, Peeters R, Vandenberghe RR. Forthcoming 2007. Remapping attentional priorities: differential contribution of superior parietal lobule and intraparietal sulcus. Cereb Cortex. doi:10.1093/cercor/bhl179.
Morecraft RJ, Cipolloni PB, Stilwell-Morecraft KS, Gedney MT, Pandya DN. 2004. Cytoarchitecture and cortical connections of the posterior cingulate and adjacent somatosensory fields in the rhesus monkey. J Comp Neurol. 469:37–69.
Morosan P, Rademacher J, Schleicher A, Amunts K, Schormann T, Zilles K. 2001. Human primary auditory cortex: cytoarchitectonic subdivisions and mapping into a spatial reference system. Neuroimage. 13:684–701.
Mountcastle VB, Lynch JC, Georgopoulos A, Sakata H, Acuna C. 1975. Posterior parietal association cortex of the monkey: command functions for operations within extrapersonal space. J Neurophysiol. 38:871–908.
Murray EA, Coulter JD. 1981. Supplementary sensory area—the medial parietal cortex in the monkey. In: Woolsey CN, editor. Multiple somatic areas. Clifton (NJ): Humana Press. p. 169–195.
Northoff G, Heinzel A, de GM, Bermpohl F, Dobrowolny H, Panksepp J. 2006. Self-referential processing in our brain—a meta-analysis of imaging studies on the self. Neuroimage. 31:440–457.
Orban GA, Claeys K, Nelissen K, Smans R, Sunaert S, Todd JT, Wardak C, Durand JB, Vanduffel W. 2006. Mapping the parietal cortex of human and non-human primates. Neuropsychologia. 44:2647–2667.
Pandya DN, Seltzer B. 1982. Intrinsic connections and architectonics of posterior parietal cortex in the rhesus monkey. J Comp Neurol. 204:196–210.
Pellijeff A, Bonilha L, Morgan PS, McKenzie K, Jackson SR. 2006. Parietal updating of limb posture: an event-related fMRI study. Neuropsychologia. 44:2685–2690.
Prado J, Clavagnier S, Otzenberger H, Scheiber C, Kennedy H, Perenin MT. 2005. Two cortical systems for reaching in central and peripheral vision. Neuron. 48:849–858.
Raichle ME, MacLeod AM, Snyder AZ, Powers WJ, Gusnard DA, Shulman GL. 2001. A default mode of brain function. Proc Natl Acad Sci USA. 98:676–682.

Ricciardi E, Bonino D, Gentili C, Sani L, Pietrini P, Vecchi T. 2006. Neural correlates of spatial working memory in humans: a functional magnetic resonance imaging study comparing visual and tactile processes. Neuroscience. 139:339–349.
Richer F, Martinez M, Robert M, Bouvier G, Saint-Hilaire JM. 1993. Stimulation of human somatosensory cortex: tactile and body displacement perceptions in medial regions. Exp Brain Res. 93:173–176.
Rizzolatti G, Matelli M. 2003. Two different streams form the dorsal visual system: anatomy and functions. Exp Brain Res. 153:146–157.
Rottschy C, Eickhoff SB, Schleicher A, Mohlberg H, Kujovic M, Zilles K, Amunts K. Forthcoming 2007. Ventral visual cortex in humans: cytoarchitectonic mapping of two extrastriate areas. Hum Brain Mapp. doi:10.1002/hbm.20348.
Rushworth MF, Behrens TE, Johansen-Berg H. 2006. Connection patterns distinguish 3 regions of human parietal cortex. Cereb Cortex. 16:1418–1430.
Sakakibara R, Fowler CJ, Hattori T. 1999. Voiding and MRI analysis of the brain. Int Urogynecol J Pelvic Floor Dysfunct. 10:192–199.
Sarkisov SA, Filimonoff IN, Kononowa EP, Preobraschenskaja IS, Kukuew LA. 1955. Atlas of the cytoarchitectonics of the human cerebral cortex. Moscow (Russia): Medgiz.
Scheperjans F, Grefkes C, Palomero-Gallagher N, Schleicher A, Zilles K. 2005. Subdivisions of human parietal area 5 revealed by quantitative receptor autoradiography: a parietal region between motor, somatosensory, and cingulate cortical areas. Neuroimage. 25:975–992.
Scheperjans F, Palomero-Gallagher N, Grefkes C, Schleicher A, Zilles K. 2005. Transmitter receptors reveal segregation of cortical areas in the human superior parietal cortex: relations to visual and somatosensory regions. Neuroimage. 28:362–379.
Schleicher A, Amunts K, Geyer S, Kowalski T, Schormann T, Palomero-Gallagher N, Zilles K. 2000. A stereological approach to human cortical architecture: identification and delineation of cortical areas. J Chem Neuroanat. 20:31–47.
Schleicher A, Amunts K, Geyer S, Morosan P, Zilles K. 1999. Observer-independent method for microstructural parcellation of cerebral cortex: a quantitative approach to cytoarchitectonics. Neuroimage. 9:165–177.
Schleicher A, Palomero-Gallagher N, Morosan P, Eickhoff SB, Kowalski T, de VK, Amunts K, Zilles K. 2005. Quantitative architectural analysis: a new approach to cortical mapping. Anat Embryol (Berl). 210:373–386.
Schleicher A, Zilles K. 1990. A quantitative approach to cytoarchitectonics: analysis of structural inhomogeneities in nervous tissue using an image analyser. J Microsc. 157(Pt 3):367–381.
Sereno MI, Huang RS. 2006. A human parietal face area contains aligned head-centered visual and tactile maps. Nat Neurosci. 9:1337–1343.
Shima K, Aya K, Mushiake H, Inase M, Aizawa H, Tanji J. 1991. Two movement-related foci in the primate cingulate cortex observed in signal-triggered and self-paced forelimb movements. J Neurophysiol. 65:188–202.
Squatrito S, Raffi M, Maioli MG, Battaglia-Mayer A. 2001. Visual motion responses of neurons in the caudal area pe of macaque monkeys. J Neurosci. 21:RC130:1–5.
Stoeckel MC, Weder B, Binkofski F, Choi HJ, Amunts K, Pieperhoff P, Shah NJ, Seitz RJ. 2004. Left and right superior parietal lobule in tactile object discrimination. Eur J Neurosci. 19:1067–1072.
Talairach J, Tournoux P. 1988. Co-planar stereotaxic atlas of the human brain. Stuttgart (Germany): Thieme.
Tuch DS, Salat DH, Wisco JJ, Zaleta AK, Hevelone ND, Rosas HD. 2005. Choice reaction time performance correlates with diffusion anisotropy in white matter pathways supporting visuospatial attention. Proc Natl Acad Sci USA. 102:12212–12217.
Uylings HB, Jacobsen AM, Zilles K, Amunts K. 2006. Left-right asymmetry in volume and number of neurons in adult Broca's area. Cortex. 42:652–658.
Uylings HB, Rajkowska G, Sanz-Arigita E, Amunts K, Zilles K. 2005. Consequences of large interindividual variability for human brain atlases: converging macroscopical imaging and microscopical neuroanatomy. Anat Embryol (Berl). 210:423–431.
Vogt BA, Vogt L, Laureys S. 2006. Cytology and functionally correlated circuits of human posterior cingulate areas. Neuroimage. 29:452–466.
Vogt O. 1911. Die Myeloarchitektonik des Isocortex parietalis. J Psychol Neurol. 18:379–390.
von Economo C, Koskinas GN. 1925. Die Cytoarchitektonik der Hirnrinde des erwachsenen Menschen. Berlin (Germany): Verlag von Julius Springer.
Watkins KE, Paus T, Lerch JP, Zijdenbos A, Collins DL, Neelin P, Taylor J, Worsley KJ, Evans AC. 2001. Structural asymmetries in the human brain: a voxel-based statistical analysis of 142 MRI scans. Cereb Cortex 11:868–877.
Wenderoth N, Toni I, Bedeleem S, Debaere F, Swinnen SP. 2006. Information processing in human parieto-frontal circuits during goal-directed bimanual movements. Neuroimage. 31:264–278.
Wolbers T, Schoell ED, Buchel C. 2006. The predictive value of white matter organization in posterior parietal cortex for spatial visualization ability. Neuroimage. 32:1450–1455.
Wree A, Schleicher A, Zilles K. 1982. Estimation of volume fractions in nervous tissue with an image analyzer. J Neurosci Methods. 6:29–43.
Zilles K, Eickhoff S, Palomero-Gallagher N. 2003. The human parietal cortex: a novel approach to its architectonic mapping. Adv Neurol. 93:1–21.
Zilles K, Schleicher A, Palomero-Gallagher N, Amunts K. 2002. Quantitative analysis of cyto- and receptor architecture of the human brain. In: Toga A and Mazziotta J, editors. Brain mapping: the methods. 2nd ed. San Diego (CA): Academic Press. p. 573–602.